# CRACK PROPAGATION IN VISCOELASTIC MATERIALS UNDER TRANSIENT LOADING WITH APPLICATION TO ADHESIVELY BONDED STRUCTURES

Thesis by

Samuel K.Y. Chang

*In Partial Fulfillment of the Requirements*

*for the Degree of*

*Aeronautical Engineer*

Graduate Aeronautical Laboratories

California Institute of Technology

Pasadena, CA 91125

December 1983

© 1983

Samuel K.Y. Chang

All Rights Reserved

## ACKNOWLEDGEMENTS

I would like to express my appreciation and grattitude to Professor W.G. Knauss for his guidance, inspiration and encouragement.

I would like to thank Clarence Hemphill and Francis Waiyaki for their help in the laboratory, and I would also like to thank Marta Nyiri for the excellent work in typing this thesis.

I dedicate this thesis to my parents, my wife, Rita, and my sister, Dora, for their prayers and supports.

# TABLE OF CONTENTS


| | |
|---|---|
| ABSTRACT | v |
| 1. INTRODUCTION | 1 |
| 2. REVIEW OF EXISTING LINEAR FRACTURE THEORY | 4 |
| 3. EXPERIMENTAL PROCEDURES | 7 |
| 3.1 Physical Description of the Method of Caustics | 7 |
| 3.2 Mathematical Description of the Method of Caustics | 7 |
| 3.3 Experimental Procedures | 18 |
| 3.4 Caustic Data Analysis | 18 |
| 3.5 Caustic Calibration | 21 |
| 3.6 Data Scattering | 24 |
| 4. RESULTS | 26 |
| 5. ANALYSIS OF EXPERIMENTAL RESULTS | 33 |
| 6. REFERENCES | 43 |
| APPENDICES | 44 |
| A. LOADING AND ENVIRONMENTAL CONTROL SYSTEM | 44 |
| B. CRACK TIP LOCATION RELATIVE TO THE CAUSTICS | 48 |

**ABSTRACT**

Linear viscoelasticity theory is applied to the fatigue problem of solids sensitive to the deformation rate. A series of experiments have been performed to investigate the range of applicability in which the theory is valid and to examine the accuracy of the theory. The experimental results are compared with an existing theory.

## 1. INTRODUCTION

Compared to 10 or 20 years ago there are many situations in engineering today where polymers are used for structural purposes. This use occurs in the civil engineering sector; in water- and gas piping constructed from Polyvinylchloride; in agriculture for irrigation and desalination purposes; in many household goods and in particular in the automotive industry. In the transportation industry polymers are widely used in automobile tires as well as in automotive body components. In the aerospace industry polymers are used to a large extent as sealants, as structural bonding agents, as well as bonding together fibers to make composite materials. The composite materials may be either of continuous, or chopped fiber type. Inasmuch as a very large percentage of engineering application of any materials encounters transient or periodic loading, it is appropriate that one give attention to the fracture behavior of these types of materials in a fatigue-type of environment.

We associate with the terminology "fatigue" the phenomenon that failure or fracture of a component occurs under a cyclic load environment at stress or load levels that are significantly lower than those that might have been sustained by the part if only a steady continuous load had been imposed. In the context of time-dependent failure of polymeric material this definition may or may not be appropriate. We know, for example, that even when steady loads are imposed on a viscoelastic material, fracture will occur in a time-delayed manner due to the slow and time-dependent growth of cracks in such a material. This phenomenon has often been associated with the term of "static fatigue". Under such circumstances it would be appropriate by the classical definition of fatigue to add into that definition some measure of a comparative time length or life so as to assess whether a cyclic or repetitive loading leads to an acceleration over the appropriate steady-state environment to which a part might be subjected.

By and large the study of fatigue in polymeric materials has been, to date, confined essentially to rigid polymers. In this connection fatigue in polymers has been treated by virtually the same methods that are normally applied to the fatigue of structural metals. Because a detailed understanding of the fatigue process in metals and also in the rigid polymers does not exist from a basic point of view, one has generally resorted to analyzing crack propagation rates under fatigue type loading as a function of the difference between maximum and minimum stress intensity factor. The resulting test curves have often come to represent essentially the fatigue material behavior instead of the S-N curves that were part of standard fatigue analysis only three decades ago.

From an engineering point of view, this may be quite an acceptable approach for dealing with the fatigue problem when the polymer is definitely in the rigid state. However, there are many situations, in particular in aerospace applications, where the material is exposed to elevated temperatures to such a degree that while substantial softening is not achieved the load duration and the fatigue environment may last long enough so that a substantial amount of damage is incurred in this elevated temperature stage. Inasmuch as at elevated temperatures polymers tend to become significantly viscoelastic, the question arises as to how the fatigue process is governed in this kind of environment when strong viscoelastic effects are present.

It appears reasonable to view the fracture behavior or failure behavior of polymeric materials from the point of view of fracture mechanics, that is, the failure behavior of these materials in the presence of preexisting cracks. In this context, it becomes reasonable therefore to inquire as to how cracks propagate in a material when strong viscoelastic material behavior is present and when the load history of the component is cyclic in nature. Inasmuch as there is at this time only an approximate theory [1] that deals with crack propagation in

polymers under cyclic conditions of loading it is appropriate to examine this problem in some detail and to do so from an experimental point of view.

At this time our foundation for understanding the propagation of cracks in viscoelastic material is based on linear viscoelastic material response. For the case of linearly viscoelastic behavior this foundation is outlined essentially in [2], while similar developments based on special material representation are covered in [3] and [4]. These developments are documented specifically for propagation theory at constant velocities, where the underlying assumption is that the crack propagation is applicable instantaneously in situations where the stresses at the tip of the crack change continuously with time. It turns out that for many situations this underlying assumption is not a serious restriction at all. However, it appears questionable to what extent these relations are applicable when the stresses change rather rapidly at the tip of the moving crack. As has been pointed out in [5], if the crack-tip stresses change rapidly compared to a length parameter characterizing a thin zone of fracturing material along the crack path, then these approximations involving constant rates of crack propagation may no longer be applicable. The fully analytical exploration of this question seems too cumbersome at this time. Rather, one would feel that it is more appropriate to examine this problem initially experimentally. Subsequent to such an experimental investigation one would then find more justification or motivation to explore particular ranges of material behavior where perhaps more suitable approximation are appropriate.

## 2. REVIEW OF EXISTING LINEAR FRACTURE THEORY

We shall summarize here briefly the developments in [2]. Consider the tip of a crack moving through a (linearly) viscoelastic material. This tip is characterized by a damage or process zone in which the material behaves non-linearly. If this zone is sufficiently small, one may make use of the linearized theory of viscoelasticity along with a line model for the process zone according to Prandtl, Barenblatt or Dugdale. The process zone needs to be incorporated to provide a length scale parameter that couples the material viscosity to a crack propagation speed. In Ref. 2 two criteria of fracture were explored: a crack-opening displacement and an energy criterion. Both gave essentially identical results. It suffices, therefore, to consider only one, the energy criterion.

The energy criterion states that the rate of work done by the unloading tractions on the displacements in the (line) plastic zone equals the rate of fracture energy absorption, which, in the simplest form, may be considered to be a constant $\Gamma$ times the crack speed $\dot{c}$. Under the assumption of *constant* crack propagation speed that criterion leads to the relation (for Poisson's ratio $\nu = 1/2$)

$$K^2 \Theta \left[ \frac{\alpha}{\dot{c}} \right] = \frac{4}{3} E_\infty \Gamma \tag{1}$$

where

$K$ = stress intensity factor

$\alpha$ = length of (line) cohesive or process zone

$\Gamma$ = rate independent fracture energy

$\dot{c}$ = rate of crack growth

$$\frac{\Theta(t)}{E_\infty} = \int_0^1 \int_\rho^1 \left\{ D\left[ \frac{\alpha}{t}(r - \rho_o) \right] - D(o) \right\} \frac{dF^+(r)}{dr}\, dr\, d\rho = D \tag{2}$$

$$F(r) = \sqrt{1-r} + \frac{1}{2}\left[ \frac{1-r}{2} \ln \frac{\sqrt{1-r}+1}{\sqrt{1-r}-1} - \sqrt{1-r}\, r \right]$$

$D(t)$ = uniaxial creep compliance

$$E_\infty = \frac{1}{D(\infty)}$$

In this context we note that eqn. (1) holds rigorously for $\dot{c}$ = const. and approximately for $\dot{c}$ const. ***provided*** (see Ref. 2)

$$\frac{|\dot{K}(t)|}{K(t)} << \frac{\dot{c}(t)}{2\alpha(t)} \tag{3}$$

This question of describing crack growth analytically by an equation like (1) was addressed in a previous analysis which was based on crack growth by small but finite increments [1] but which did not limit itself to the cases allowed by [2]. The net result of that analysis was that if viscoelastic transients become important (i.e. if the equation (3) above is violated) then crack propagation per cycle should occur more rapidly than if only the quasi-steady relations (1) is involved ($\dot{c}$ = const.). Inasmuch as equation (1) is much easier to apply than the work in Ref. 1 one may raise the question whether the deficiency associated with violation of (3) is really important: After all, a problem may exist only near $\dot{c}$=0, so that the total amount of crack growth accumulated near the "crack growth boundary"[1] is very small to begin with and thus possibly an important contribution to the total crack length. The constraint (3) is always violated when a crack tip experiences loading that passes through the limit for possible crack propagation: Below and at this limit $\dot{c} = 0$ but $\dot{K}(t) \neq 0$; the same is true for conditions above this limit where both $\dot{K}$ and $\dot{c}$ exceed zero, but still close enough to the propagation limit so that the order relation is violated. The question arises thus to what extent equation (1) can represent crack growth under conditions when the propagation boundary is passed, particularly passed repeatedly as in a cyclic history. It is possible that equation (1) would be more powerful than the analytical estimates would indicate. It appears, however, reasonable to expect

1. Crack growth is not possible if the stress intensity is below a certain value say $K^*$; above $K^*$ crack growth occurs. We call $K^*$ the crack growth boundary.

that the range of validity of (1) is somehow limited by the inequality (2) and that the argument of "small crack growth contribution" means that the propagation boundary may only extend the range of validity for (1) somewhat.

In view of this situation it is appropriate to examine the crack growth behavior under transient rather than steady loading conditions experimentally. The results of such an investigation would then provide further input to analytical formulations that elucidate the behavior of crack growth under rather arbitrary transient loading histories. Because of its technical importance as well as the ease with which small crack growth can be accumulated over many cycles into a readily measurable quantity, cyclic deformation histories seem to be well suited to this study.

For later reference it should be pointed out that evaluation of crack growth under transient load histories, if governed by equation (1), was carried out in considerable detail in [6]; this study will serve as a guide and reference against which the experimental results can be compared.

We proceed next to a description of the experimental set-up and analysis of the experimental technique (caustics). Following these developments we turn to the recording and then analysis of the experimental results.

## 3. EXPERIMENTAL PROCEDURES

For measuring the stress intensity factor K(t) and the crack length c(t) in the same time frame, the method of caustics is adopted. This method, also called "shadow spot method", or "the method of shadow pattern", was recognized by Schardin and analyzed by Mannog in 1959. Through the works of Theocaris, Kalthoff and others (Knauss, Rosakis, Kim, Ravi-Chandar) this method is not only useful for elastic materials, but also for viscoelastic ones [7].

### 3.1 Physical Description of the Method of Caustics

When a beam of parallel light is incident normally on a stress free plate of transparent material, the beam of light just passes through. However, if there is a crack in the plate, say under Mode-1 loading, the light rays will be deflected, particularly in the crack tip region. Due to the stress field in the material the index of refraction of the material will change. Also, around the crack tip the shape of the plate surface is altered. Both effects will cause the transmitted light to deviate from the original straight path. By the Maxwell-Neumann elasto-optical law the refraction index is decreased; this fact plus that of the non-homogeneous surface deformation makes the crack tip act like a divergent lense (cf. Figure 3.1). The light around the crack tip is deflected outward so that on an image plane the area around the crack tip is devoid of light and a dark spot is formed. A photograph of a test situation is shown in Figure 3.2.

### 3.2 Mathematical Description

Consider the optical arrangement in Figure 3.3 of a cracked plate represented by the object plane and a viewing plane or image plane IP is located at a distance $z_o$ from and parallel to the object plane. Let a light ray be incident at point P on the object plane with coordinates $P = P(r, \varphi)$. If the light were not deflected, it would intersect the image plane at the point P'. Actually the ray will

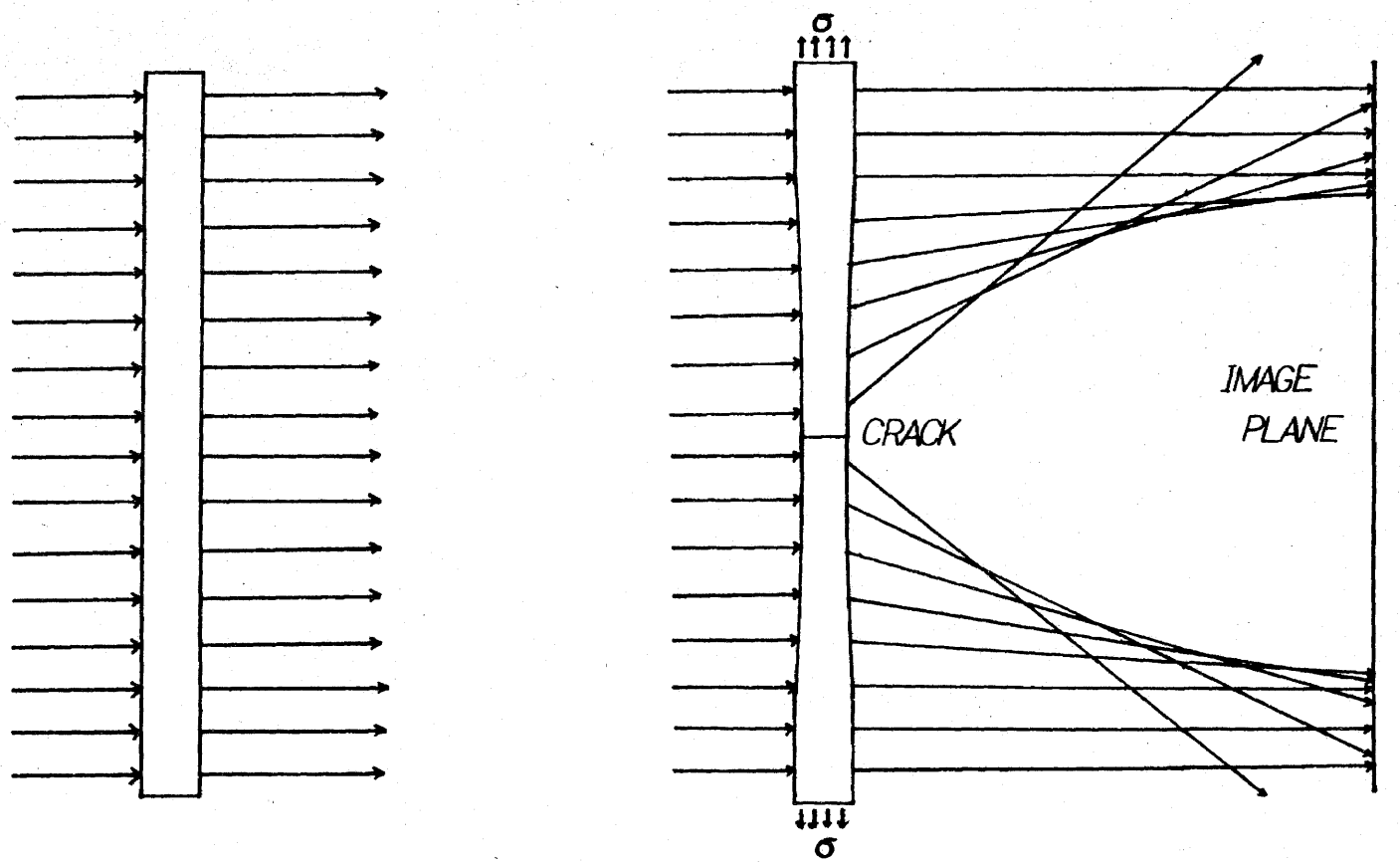


**Figure 3.1** Effect of crack tip stresses on light paths.

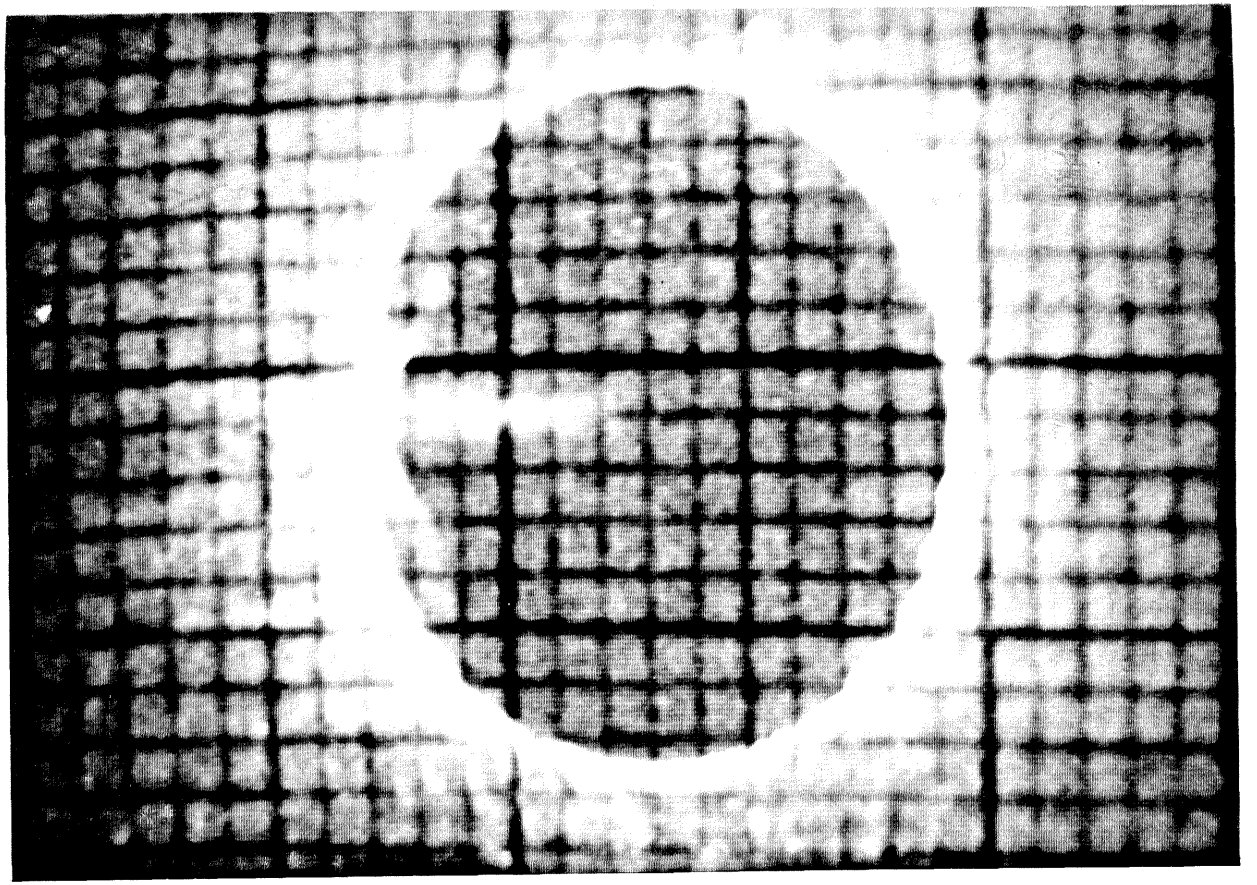

**Figure 3.2** Photo of a caustic spot (Solithane 113 (50/50)).

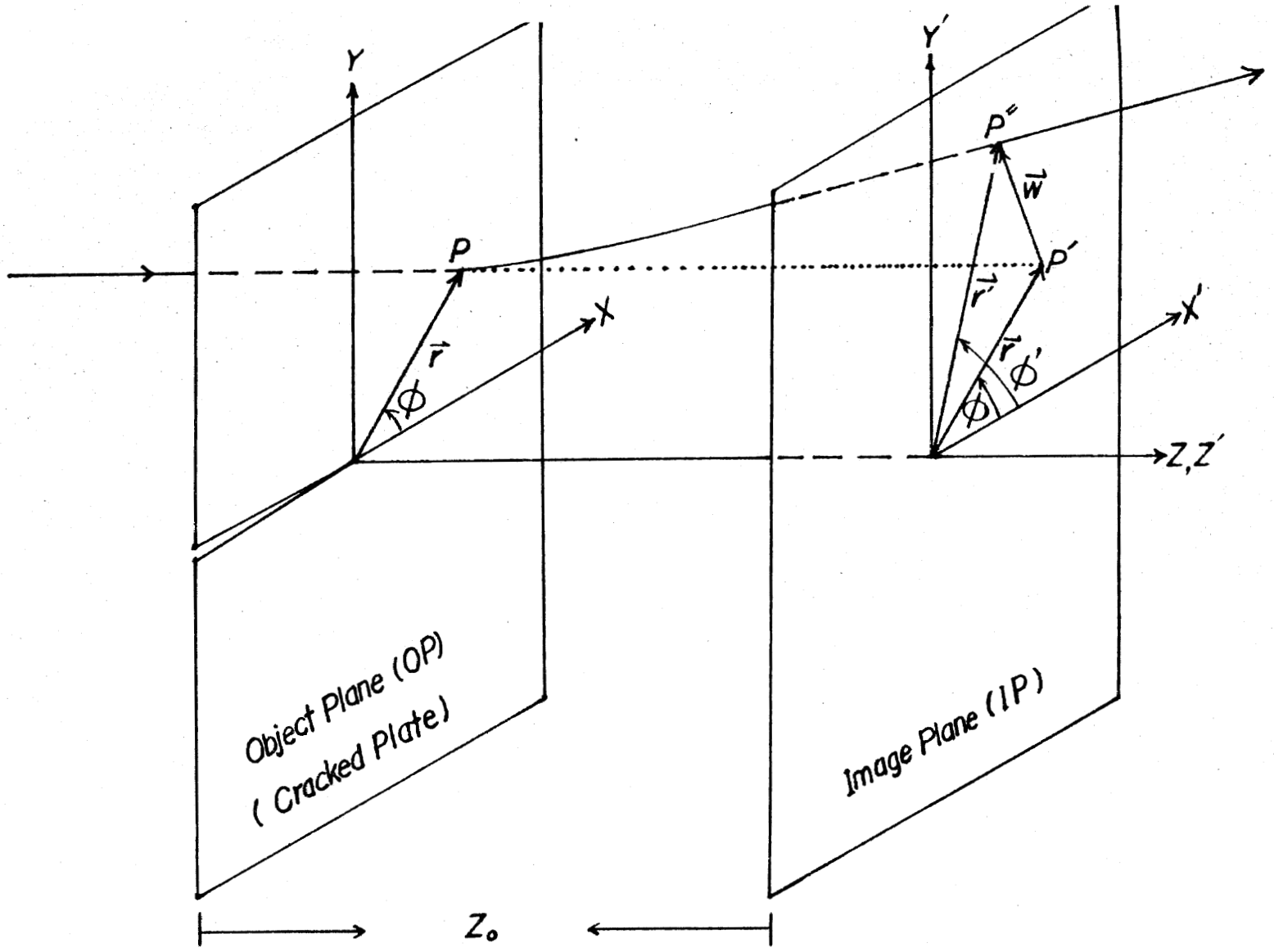


**Figure 3.3** Optical paths for development of caustic.

be deflected to intersect the image plane at the point P''. By the geometry in Figure 3.3, we have then

$$\vec{r}' = \vec{r} + \vec{w}(r,\varphi) \tag{1}$$

where $\vec{w}(r,\varphi)$ is a deviation vector. Applying the theory of the eikonal one has

$$\vec{w}(r,\varphi) = z_o \nabla \left( \Delta s(r,\varphi) \right) \tag{2}$$

where $\Delta s(r,\varphi)$ is the total change in light path orientation as the ray passes through the material. By the Maxwell-Neumann stress optic law and Hooke's law one has for $\Delta s$

$$\Delta s = h \cdot \lambda \left[ (\sigma_1 + \sigma_2) \pm (\sigma_1 - \sigma_2) \cdot p \right] \tag{3}$$

where the following definitions hold

$$\lambda = \frac{\lambda_1 + \lambda_2}{2} - (n-1)\frac{\nu}{E}$$

$$p = \frac{\lambda_1 - \lambda_2}{\lambda_1 + \lambda_2 - 2(n-1)\frac{\nu}{E}}$$

$h =$ thickness of the plate

$\lambda_1, \lambda_2 =$ stress optical constants

$\sigma_1, \sigma_2 =$ principal stresses

$E =$ modulus of elasticity

$\nu =$ Poisson's ratio

$n =$ index of refraction

If $\lambda_1 \neq \lambda_2$ the material is called optically anisotropic, or birefringent. The consequence is that $p \neq 0$ and therefore $\Delta s$ has two values. Therefore there will be two vectors $\vec{w}$, i.e. there will be two caustics. It turns out, ***practically*** speaking, that Solithane 113 (50/50) is optically isotropic, i.e. $\lambda_1 = \lambda_2$, and $p = 0$, so that only one caustic is observed. For optically isotropc materials

$$\Delta s = h \cdot \lambda(\sigma_1 + \sigma_2) \,. \tag{4}$$

For viscoelastic and optically isotropic materials the corresponding relation is in the form of a convolution, namely

$$\Delta s = h \cdot \lambda \;\; * \;\; \sigma \tag{5}$$

where the star (*) notation signifies the Stieltje's Integral. Thus, the optical path change within the material is a function of the stress and deformation history. Recall that in linear elasticity the stresses near the crack tip (in the object plane) are

$$\sigma_x = \frac{K_I(t)}{\sqrt{2\pi r}} \cos\frac{\varphi}{2} (1 - \sin\frac{\varphi}{2} \sin\frac{3\varphi}{2}) \; + \cdots \tag{6a}$$

$$\sigma_2 = \frac{K_I(t)}{\sqrt{2\pi r}} \cos\frac{\varphi}{2} (1 + \sin\frac{\varphi}{2} \sin\frac{3\varphi}{2}) \; + \cdots \tag{6b}$$

$$\tau_{xy} = \frac{K_I(t)}{\sqrt{2\pi r}} \cos\frac{\varphi}{2} \sin\frac{\varphi}{2} \cos\frac{3\varphi}{2} . \qquad + \cdots \tag{6c}$$

It follows that the stress invariant $\sigma_1 + \sigma_2 = \sigma_x + \sigma_y \equiv \sigma$ is

$$\sigma = \frac{K_I(t)}{\sqrt{2\pi r}} 2\cos\frac{\varphi}{2} . \tag{7}$$

Therefore equation (1) becomes, with the help of Equations (5) and (6)

$$\vec{r}' = \vec{r} + dz_o(\lambda(t) \;\; * \;\; K_I(t)) \, \nabla \, (\sqrt{\frac{2}{\pi r}} \cos\frac{\varphi}{2}) \tag{8}$$

which, in Cartesian components is equivalent to

$$x' = r\cos\varphi - dz_o[\, \lambda(t) \;\; * \;\; K_I(t) \,] \, \frac{1}{\sqrt{2\pi}} r^{-\frac{3}{2}} \cos\frac{3}{2}\varphi \tag{9a}$$

$$y' = r\sin\varphi - dz_o[\, \lambda(t) \;\; * \;\; K_I(t) \,] \, \frac{1}{\sqrt{2\pi}} r^{-\frac{3}{2}} \sin\frac{3}{2}\varphi \,. \tag{9b}$$

We next observe that in the image plane, the caustic is the envelope of all singular points for equations (9a) and (9b). Thus the caustic can be expressed by the

singularity condition (J = Jacobian of x', y' with regard to r, $\varphi$)

$$J = \frac{\partial x'}{\partial r}\frac{\partial y'}{\partial \varphi} - \frac{\partial x'}{\partial \varphi}\frac{\partial y'}{\partial r} = 0 . \tag{10}$$

If we define the curve $r(\varphi)$ in the object plane from which the rays fall on the caustic curve in the image plane as $r = r_s(\rho)$, then this relation yields that

a. The radius $r_s$ is independent of $\rho$; i.e., the curve is a circle with center at the crack tip; this curve is called the "initial curve."

b. the radius $r_s$ of the initial curve is given by

$$r_s = \left\{ \frac{3}{2} \frac{hz_o}{\sqrt{2\pi}} [\, \lambda(t) \;*\; K_I(t) \,] \right\}^{\frac{2}{5}} \tag{11}$$

The image of that initial curve (circle), i.e., the caustic is given by equation (9) together with (11) as

$$X' = r_s(\cos\varphi + \frac{2}{3}\cos\frac{3}{2}\varphi) \tag{12a}$$

$$Y' = r_s(\sin\varphi + \frac{2}{3}\sin\frac{3}{2}\varphi) \tag{12b}$$

A plot of equations (12) is given in Figure 3.4 for a particular time when $r_s$ is some constant. Now define $D=2Y'_{max}$ (cf. Fig. 3.4). Then

$$\begin{aligned} D &= 2 \cdot \max [\, r_s ( \sin\varphi + \frac{2}{3}\sin\frac{3}{2}\varphi ) \,] \\ &= 2r_s \max ( \sin\varphi + \frac{2}{3}\sin\frac{3}{2}\varphi ) \\ &= r_s f \end{aligned} \tag{13}$$

where

$$f = 2 \cdot \mathrm{Max}(\sin\varphi + \frac{2}{3}\sin\frac{3}{2}\varphi)$$

Use of (13) together with (11) renders the convolution relation

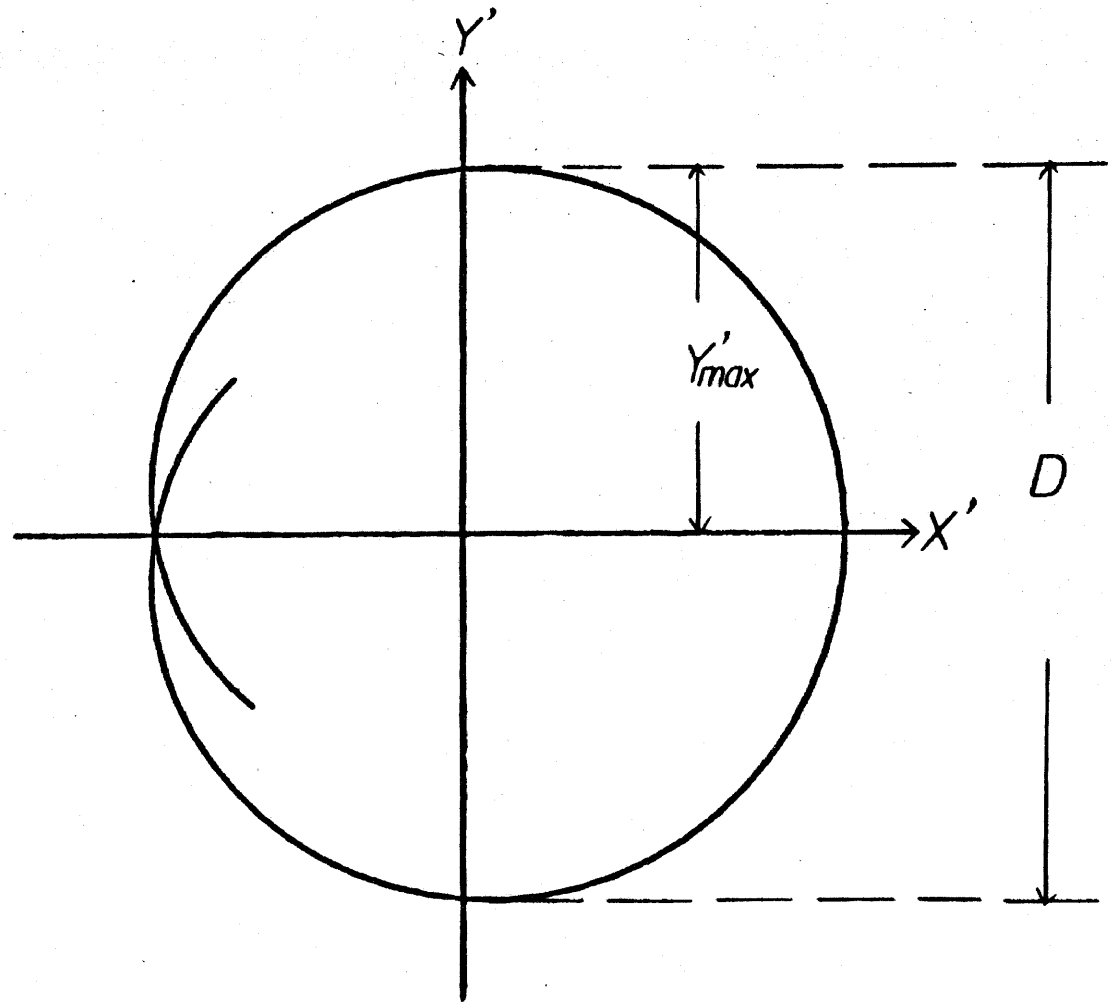


**Figure 3.4** Computed caustic.

$$K_I(t) * \lambda(t) = \frac{2\sqrt{2\pi}}{3f^{\frac{5}{2}} \cdot h \cdot z_o} D^{\frac{5}{2}} \tag{14}$$

Thus by measuring the "caustic diameters" D(t) as a function of time, the corresponding stress intensity factor K can be calculated from (14).

The determination of K requires the solution of an (convolution) integral equation; this is not a trivial matter, in general. For further work here we therefore make use of results in [7] which establishes an excellent approximation for the test material and load histories used in this investigation. In [7] it was established that essentially elastic conditions prevail for times longer than $10^{-1}$ min (cf. Figure 3.5) at a temperature of 0°C. It was also shown that the time-temperature equivalence principle holds. With this information it is possible to determine those conditions on temperature and test frequency for which elastic rather than fully viscoelastic conditions prevail. With this information one is able to construct a curve of frequency vs. temperature that "separates" the elastic from the viscoelastic behavior[1]

This relation is shown in Figure 3.6 along with the test conditions (as points) used in the later experiments. It is clear from these considerations that the caustic data gathered in the subsequent tests can be used to compute the stress intensity factor from the elastic solution represented by equation (15) where the constant λ (definition following equation (3)) incorporates the long time or rubbery Young's modulus of the test material.

$$K_I(t) = \frac{2\sqrt{2\pi}\, D(t)^{\frac{5}{2}}}{3f^{\frac{5}{2}} h z_o \lambda} \tag{15}$$

1. This curve shown is, of course, a sharp demarcation instead of the "region" in which viscoelastic behavior is weak. For this reason the curve is adjoined by a shaded region, in which viscoelasticity behavior is minimal.

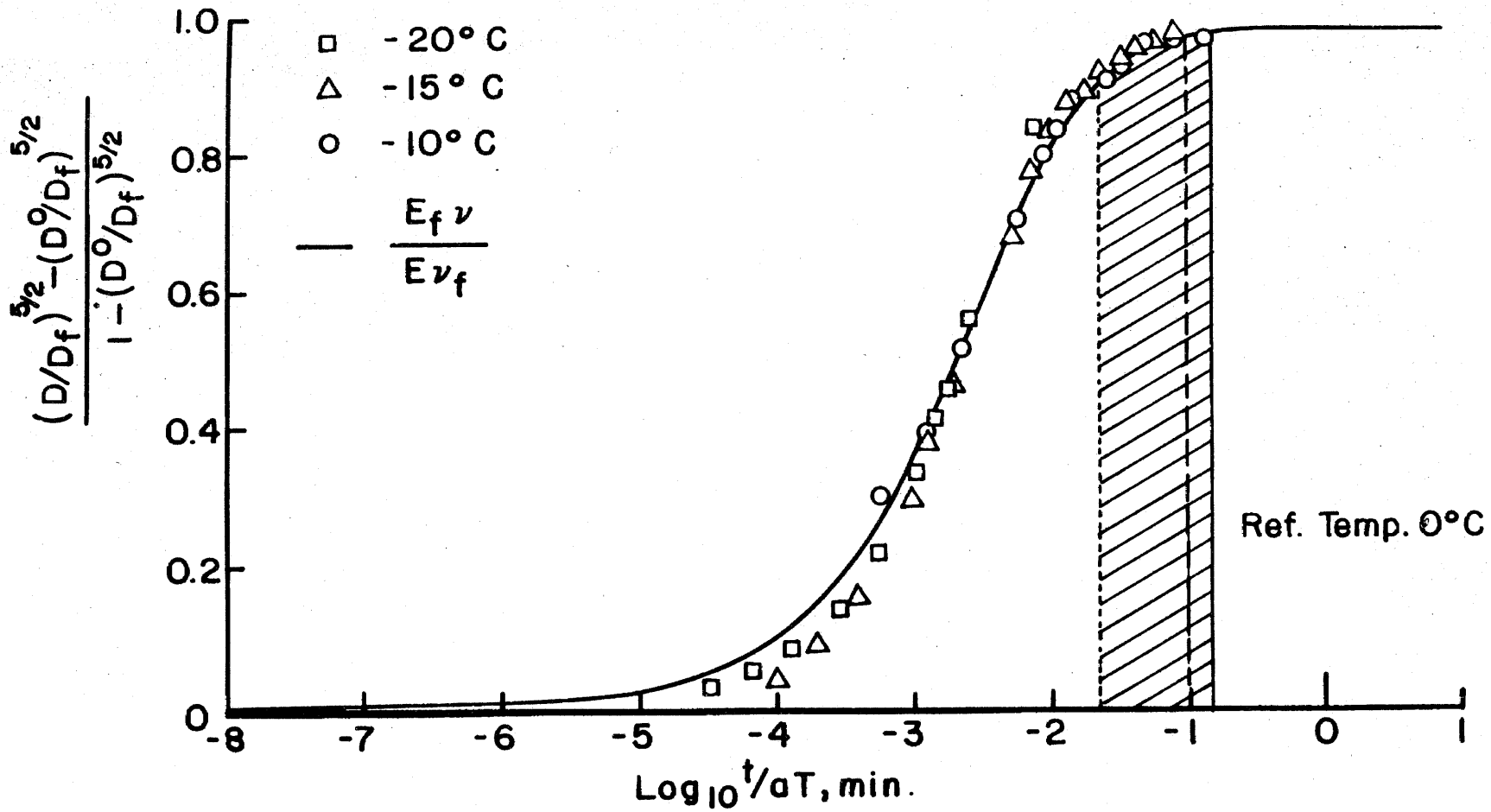


CAUSTIC CREEP CURVE

**Figure 3.5** Experimental and analytical dependence of the caustic diameter on time for step loading (from Ref. 7).

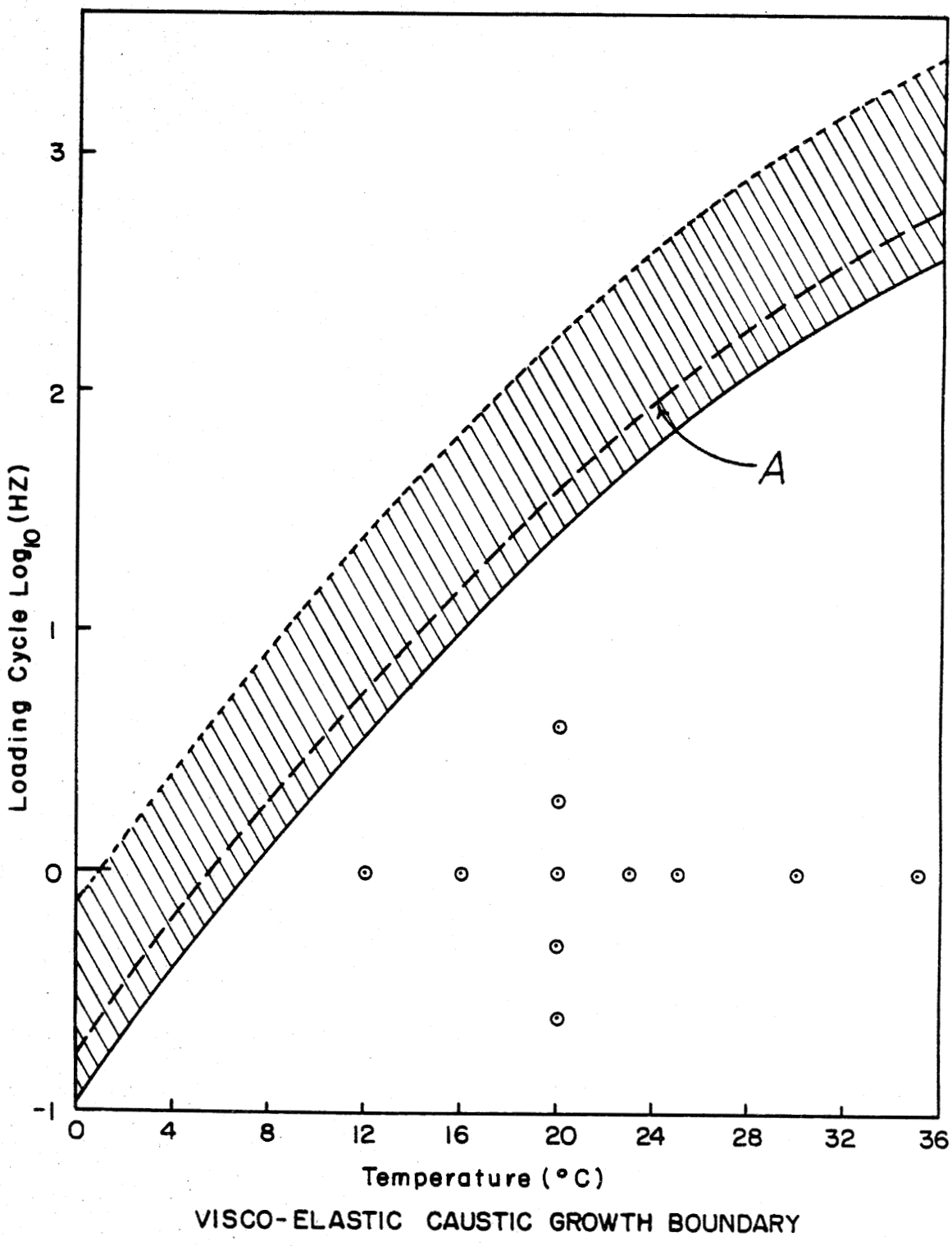


**Figure 3.6** Curve A corresponds to $10^{-1}$ minutes in Figure 3.5

It should be mentioned that we shall be interested in a moving crack, while the caustic relation (15) corresponds to a stationary crack. However, the crack will be moving so slowly that dynamic effects are irrelevant so that the present analysis is totally adequate to deal with the later test situations.

### 3.3 Experimental Procedure

We shall attempt to study crack growth as a function of the *maximum* stress intensity during any cycle. Thus it will be necessary to record the maximal caustic diameter D during any cycle. This is accomplished in the set-up shown in Figure 3.7.

A Spectra Physics Model 120 Laser shines light through a spatial filter and beam expander onto the crack tip of a specimen supported in a (servo-hydraulic) test machine. The image plane is formed by a translucent piece of paper with mm rulings . This arrangement allows virtually continual monitoring of the caustic size by means of a video camera and recorder. Data is reduced later from the video tapes.

### 3.4 Caustic Data Analysis

In order to avoid buckling of the specimen, only tension-tension cycling was performed such that there was always tension on the specimen. The lowest value of the caustic was used to locate the tip of the crack relative to the boundary. It turns out that the location of the crack tip is determined relative to the caustic by the discussions shown in Figure 3.8. The computation of these dimensions are shown in Appendix B. The diameter of the caustic under maximum load is measured (off the video-play back) as a function of crack length in the same cycle. It will be noted from equation (15) that the stress intensity factor can be determined if all the parameters characterizing the material as well as the experimental set-up are known. It turned out that some of this informations was

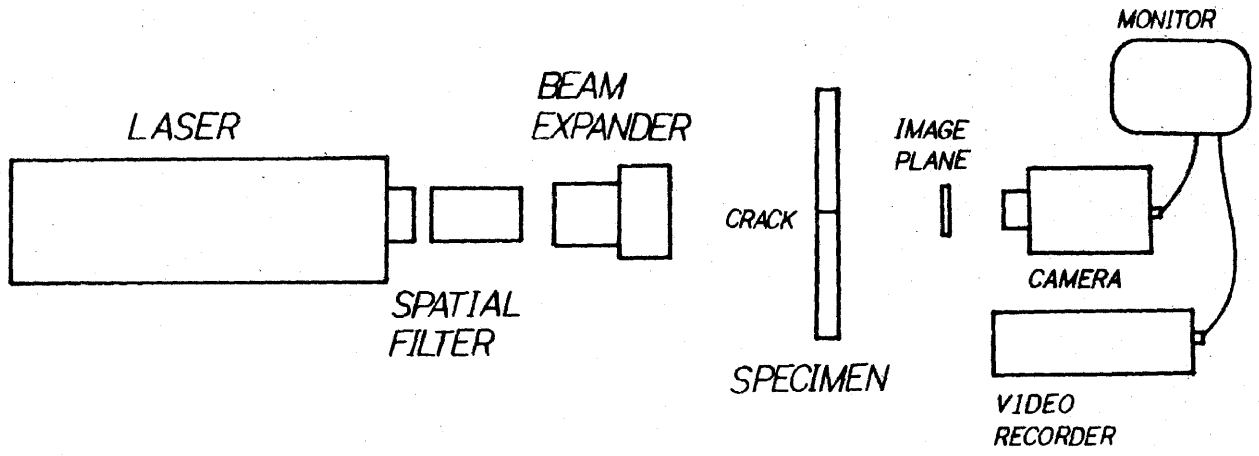


**Figure 3.7** Experimental set-up for cyclic crack growth experiment.

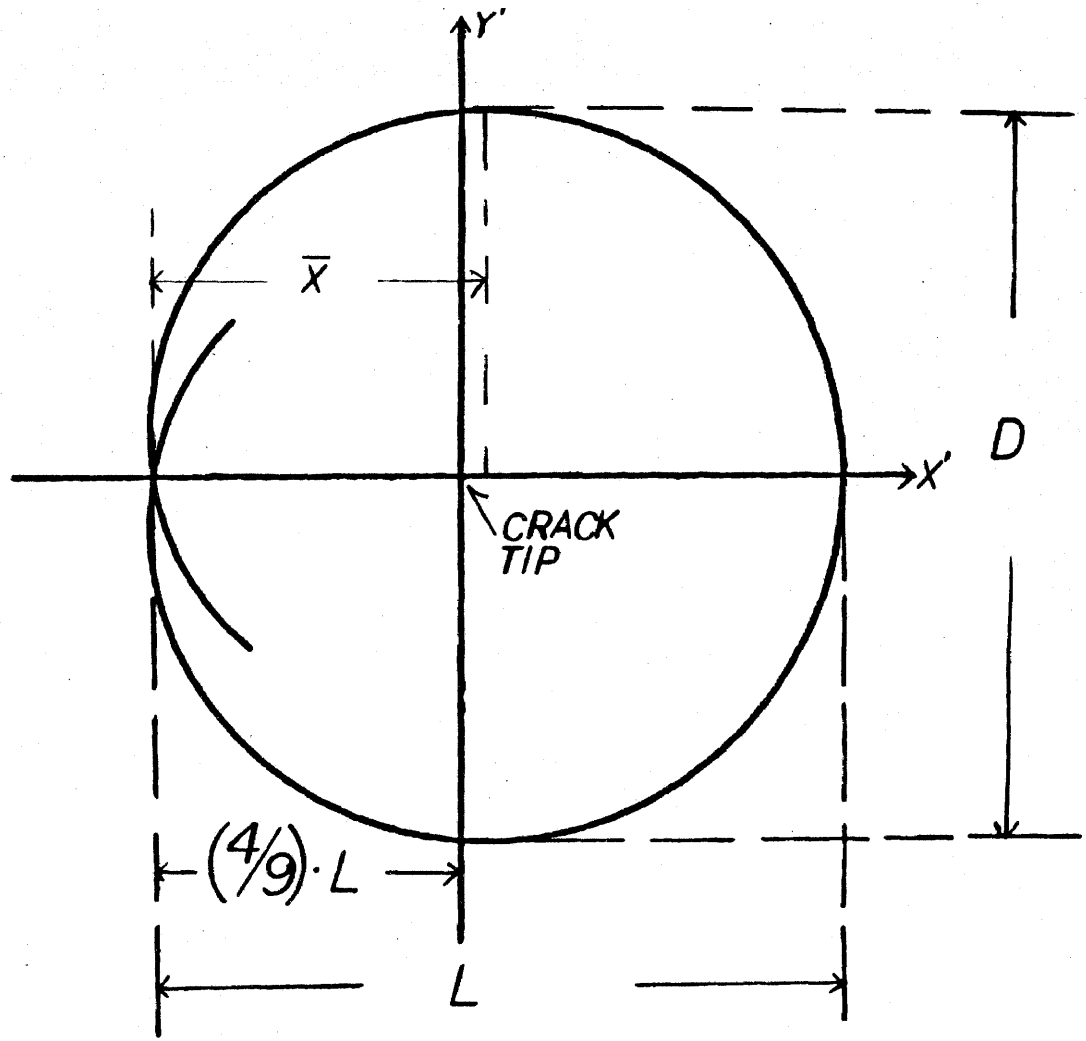


**Figure 3.8** Location of crack tip relative to caustic.

not available, in particular the stress-optic coefficient for Solithane 113. In terms of equation (15) this means that the parameter $\lambda$ is not known. The determination of the stress-optic coefficient is not a trivial matter. Therefore it was deemed more time-efficient to ascertain this parameter $\lambda$ in a separate calibration process, rather than the stress optic coefficient.

**3.5 Caustic Calibration**

To this end a typical specimen (cf. Figure 3.9) is mounted in an Instron test machine (screw-type loading device) with a C-type load-cell in the 0-20 lb range. Under a given load the caustic is recorded and the corresponding crack length noted. Using the analytical results for this geometry (infinitesimal elasticity solution [8]), one notes, as for example from equation (15), that the 5/2 power of the caustic diameter D is linearly proportional to the stress intensity factor. Thus, if one plots $D^{\frac{5}{2}}$ against the theoretically determined stress intensity factor one should obtain a straight line. This stress intensity factor would be based on the conditions prevailing in the experiment (load and crack length as well as the rest of the geometry). As can be seen from Figure 3.10, the resulting experimentally determined points fall very neatly along a straight line. A best straight line fit to this data, is then accomplished as shown; this line determines the value of $\lambda f^{5/2}$ in equation (15) and, by deduction, the long-time value of the stress-optic coefficient. It should be remarked that the experimental points in Figure 3.10 are obtained by varying the applied stress as well as by varying the crack length for computing the "theoretical" value of the stress intensity factor.

For purposes of completeness let us record here the pertinent equation for this computation. From [8] we have for the stress intensity factor (Mode-I)

$$K_I = 1.1215\sigma \sqrt{\pi a} \cdot F(\frac{H}{b})$$

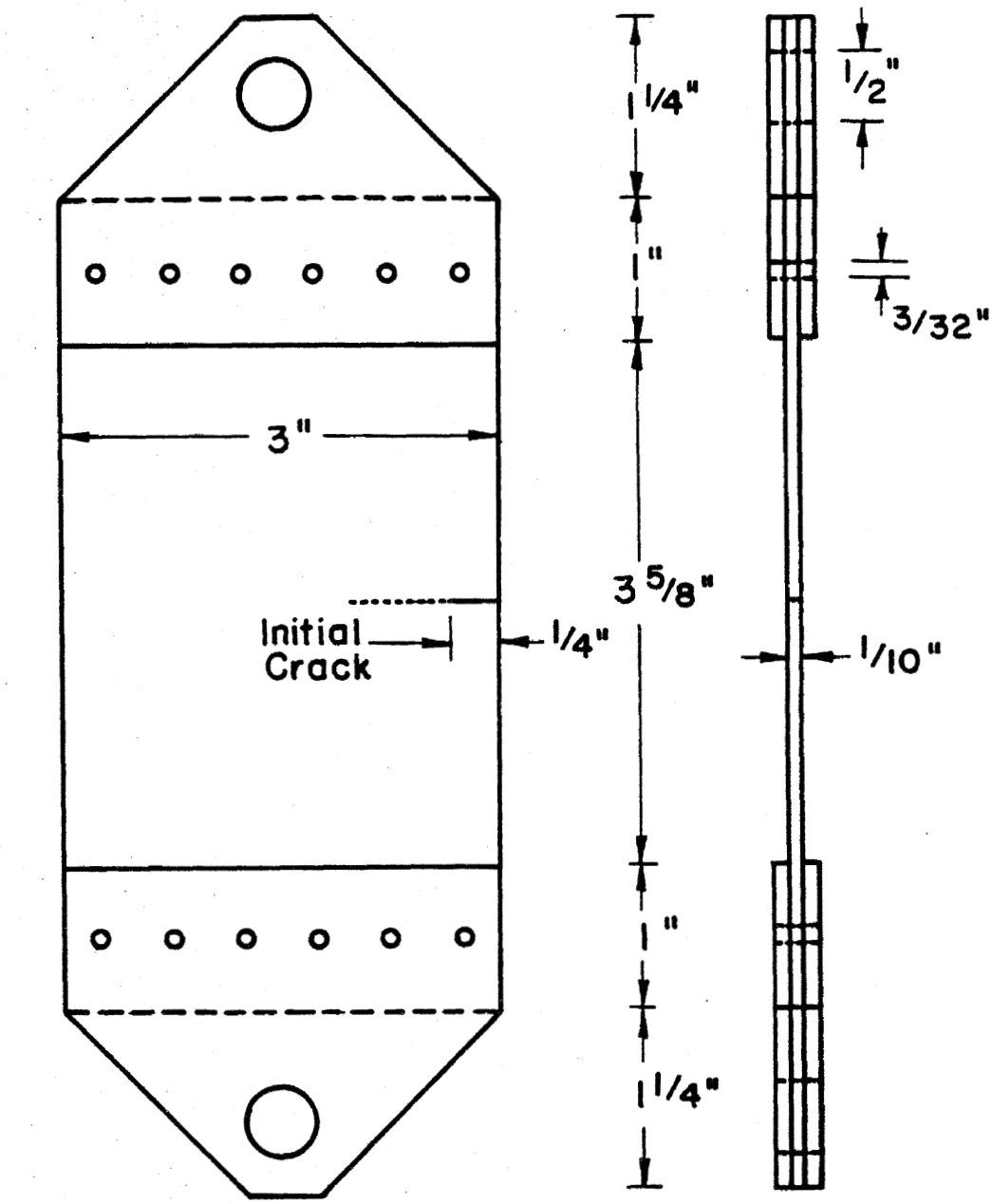


GEOMETRY CONFIGURATION OF THE TESTING SAMPLE

**Figure 3.9** Geometry configuration of the testing sample.

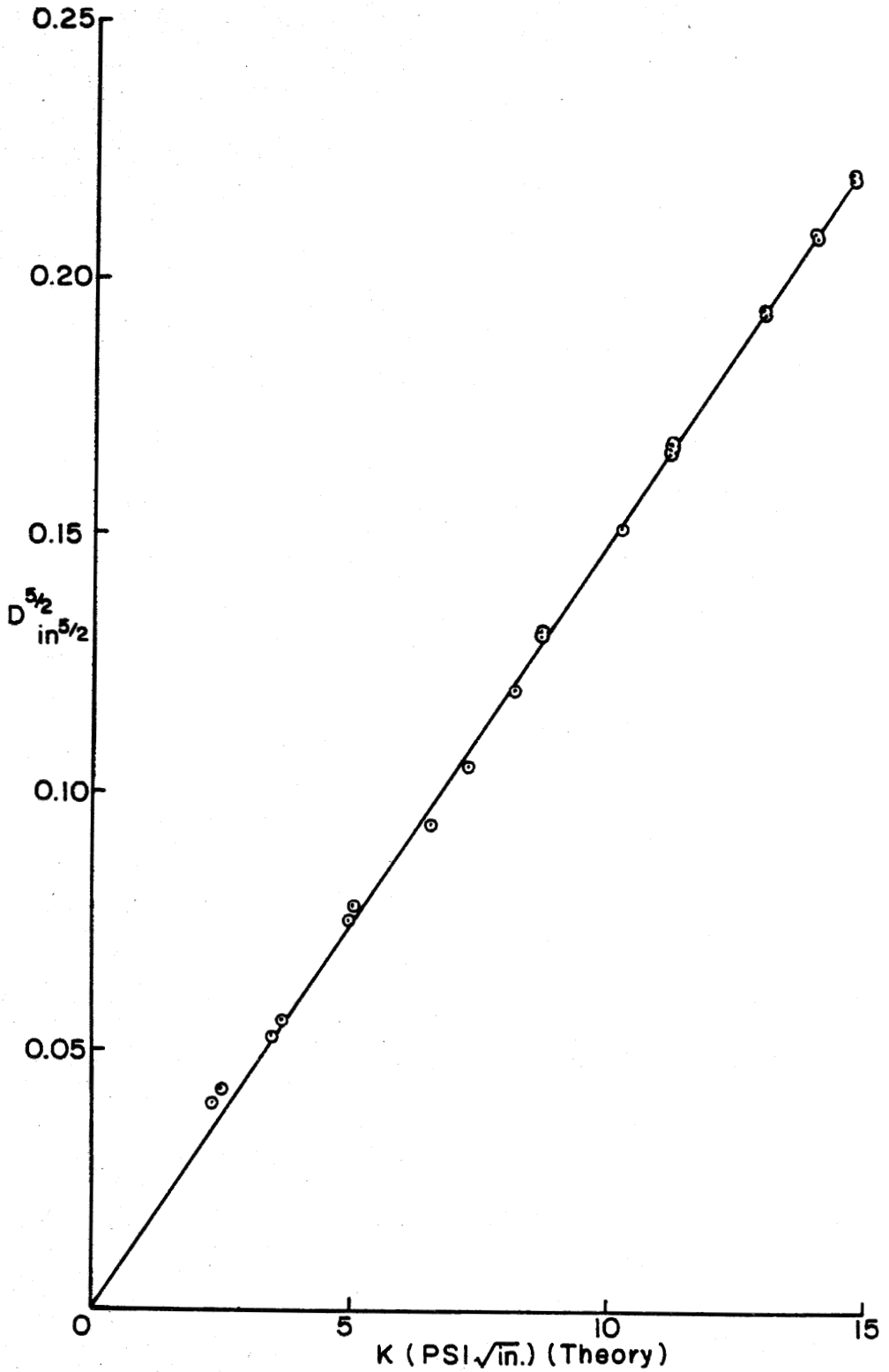


**Figure 3.10** Calibration of the caustic parameter λ.

where $\sigma$ is the average grip stress and (H,b) are as defined in the inset of Figure 3.11. The function $K_I/K_o = 1.1215 \cdot F(\frac{H}{b})$ is given in that figure for two end conditions that do or do not allow for rotation of the grips. In the present experiments no rotation was allowed; hence only the appropriate interpolated curve for h/b = 0.67 shown in Figure 3.11 was used.

Before proceeding to evaluate the fatigue data it is worth while to mention why the photoelastic method was not used. It turns out that with a specimen thickness of 2.5 mm (0.1 inch) the photoelastic method was no more sensitive or accurate than the caustic method. In this situation the caustic method is easier to use because only a single parameter must be measured (D) while in the photoelastic method field data needs to be analyzed for a best fit of the crack-tip stress field to existing photo-elastic figures [9].

**3.6 Data Scatter**

A brief note is in order regarding data scatter. It will be noted that there is very little data scatter present in all the subsequent measurements. This fact is a direct consequence of the care with which the maximum stress intensity was determined in each cycle as well as the how the crack length was determined. The latter was measured under conditions when the crack was almost closed (lowest stress in any cycle). These simple rules produced very consistent data subject only to variations in material properties along the crack path, which variations could give rise to data scatter measurements of the crack propagation rate. That this did not happen to any sizable degree testifies only to the uniformity of test material.

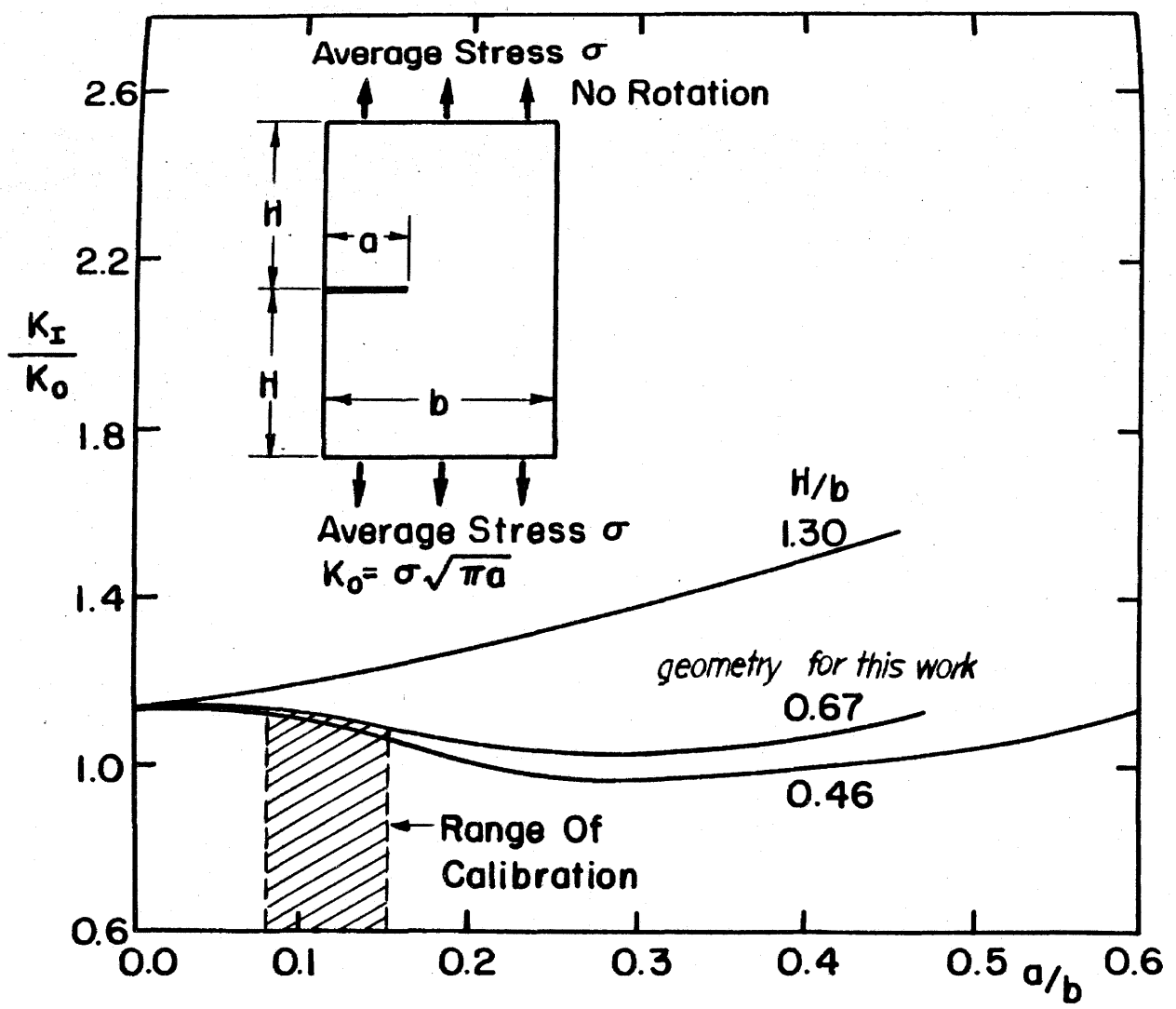


**Figure 3.11** Computed stress intensity factor for test geometry (Ref. 8).

## 4. RESULTS

In order to explore the applicability of the crack propagation equation (1) it is necessary to perform tests over a matrix of frequencies and temperature. If the material behaves in a thermorheologically simple manner, it would be sufficient to perform these tests at only one frequency and several temperatures, or at one temperature and several frequencies. Although in previous, steady-state test the crack propagation behavior followed essentially thermorheologically simple behavior we do not know for certain what the effect of cycle frequency is on generating heat at the crack tip and thus influence the crack growth rate in this secondary manner. For this reason two sets of data were taken: in one - let us call it Set I - the temperature varied but the frequency was always 1 Hz while in the second set - for discussion purposes denoted by Set II - the frequency varied and the temperature remained constant at 20°C. These test points are shown graphically in the plot of the viscoelastical caustic boundary (cf. Figure 3.6).

For any of these tests one records the length of the crack as a function of the number of cycles as well as the corresponding instantaneous stress intensity factor. For Set I (varied temperature at 1 Hz) the data are recorded in Figure 4.1 and 4.2, while for Set II (varied frequency at 20°) they are shown in Figures 4.3 and 4.4. Note the relatively small amount of data scatter. The crack length data in Figures 4.1 and 4.3 are then differentiated numerically by the five-point Lagrange method [10,11]. Differentiation is accomplished with respect to the number of cycles (as a continuous variable), though Set I leads directly to the time derivative because the frequency is one Hz; the results of this differentiation are given in Figures 4.5 and 4.6.

Upon cross-plotting the data from Figures 4.2 and 4.5 one eliminates the

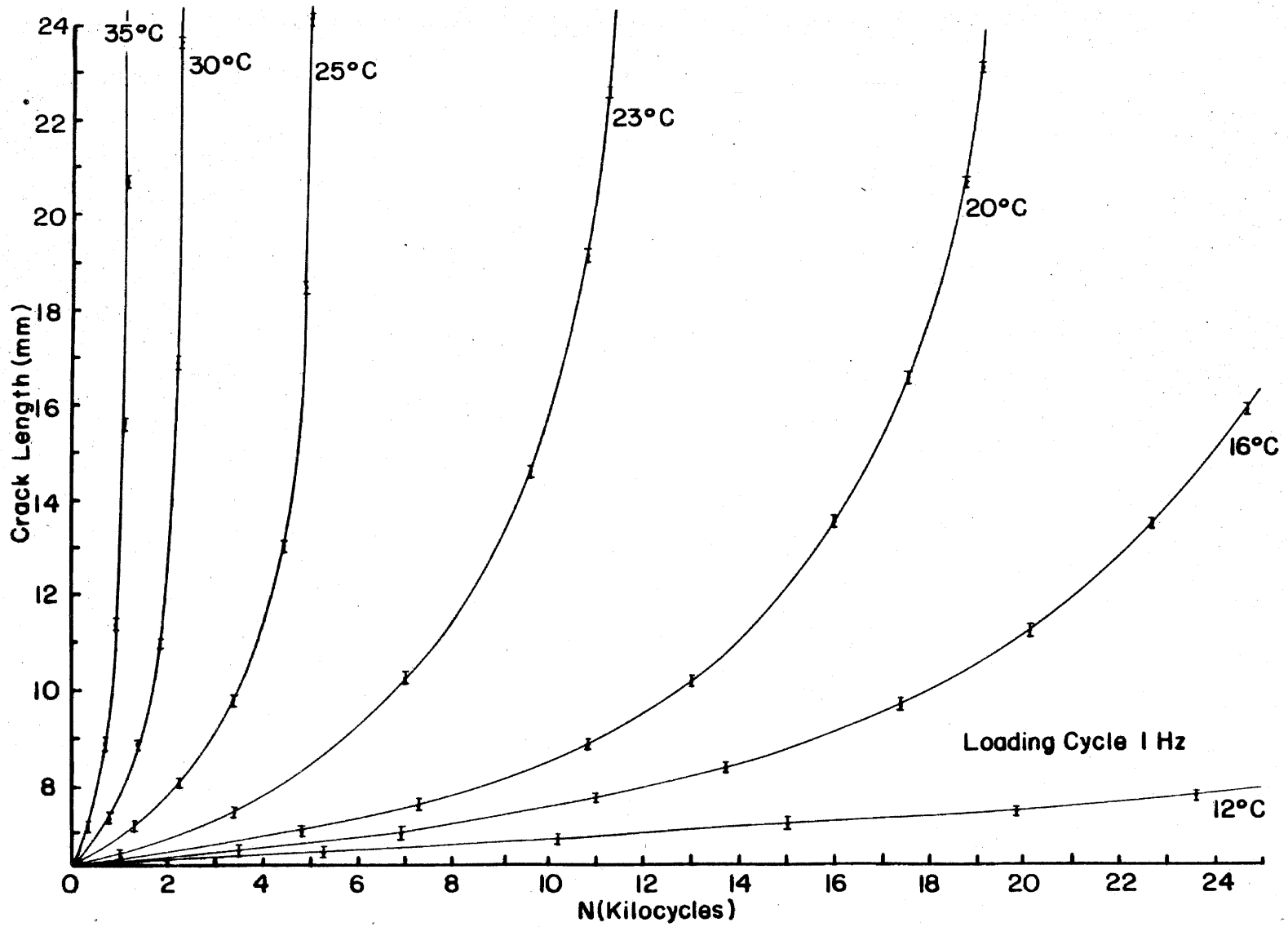


**Figure 4.1** Crack length recorded as a function of the number of cycles in different temperatures.

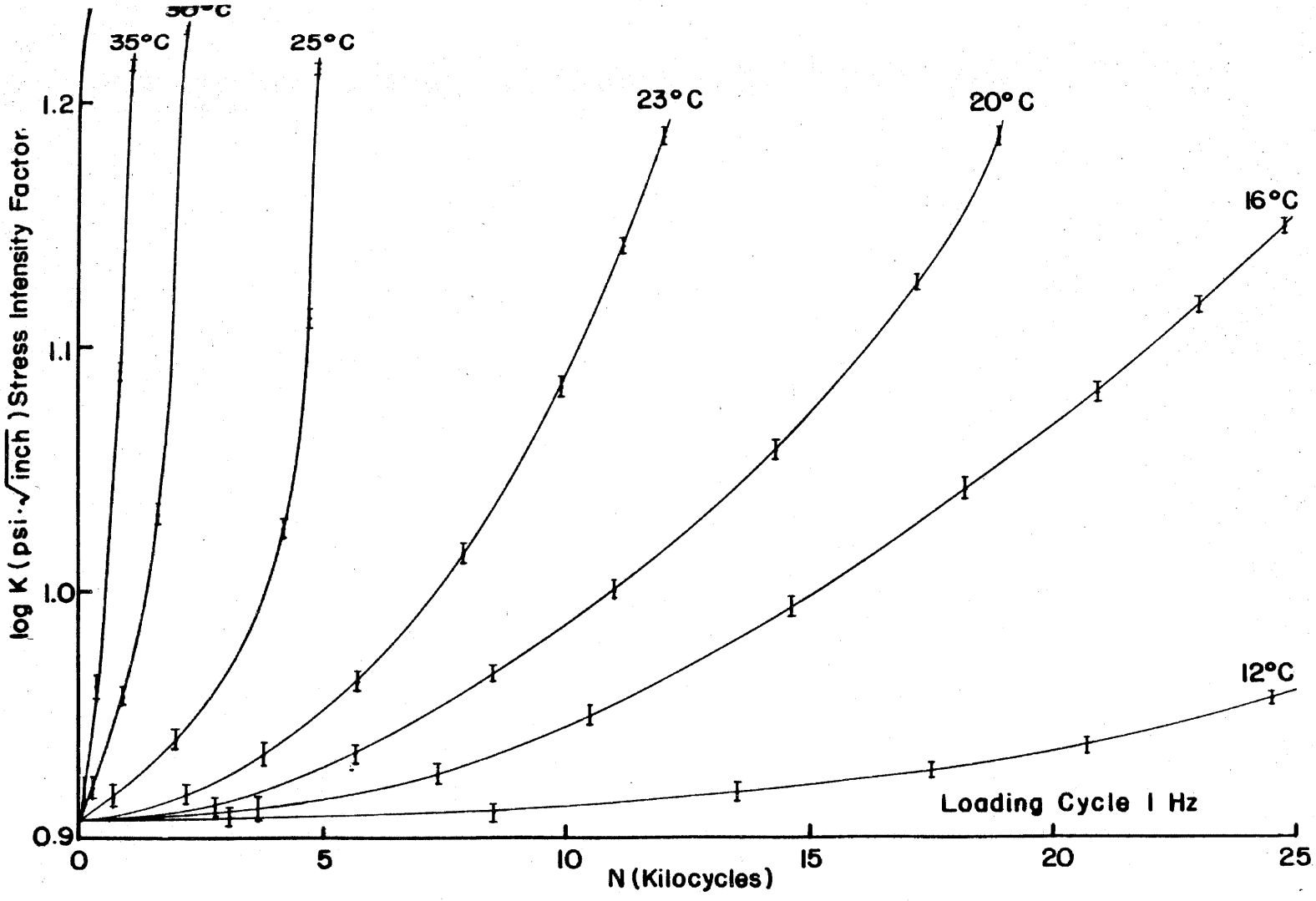


**Figure 4.2** The log values of stress intensity factors $K_I$ recorded as a function of the number of cycles in different temperatures.

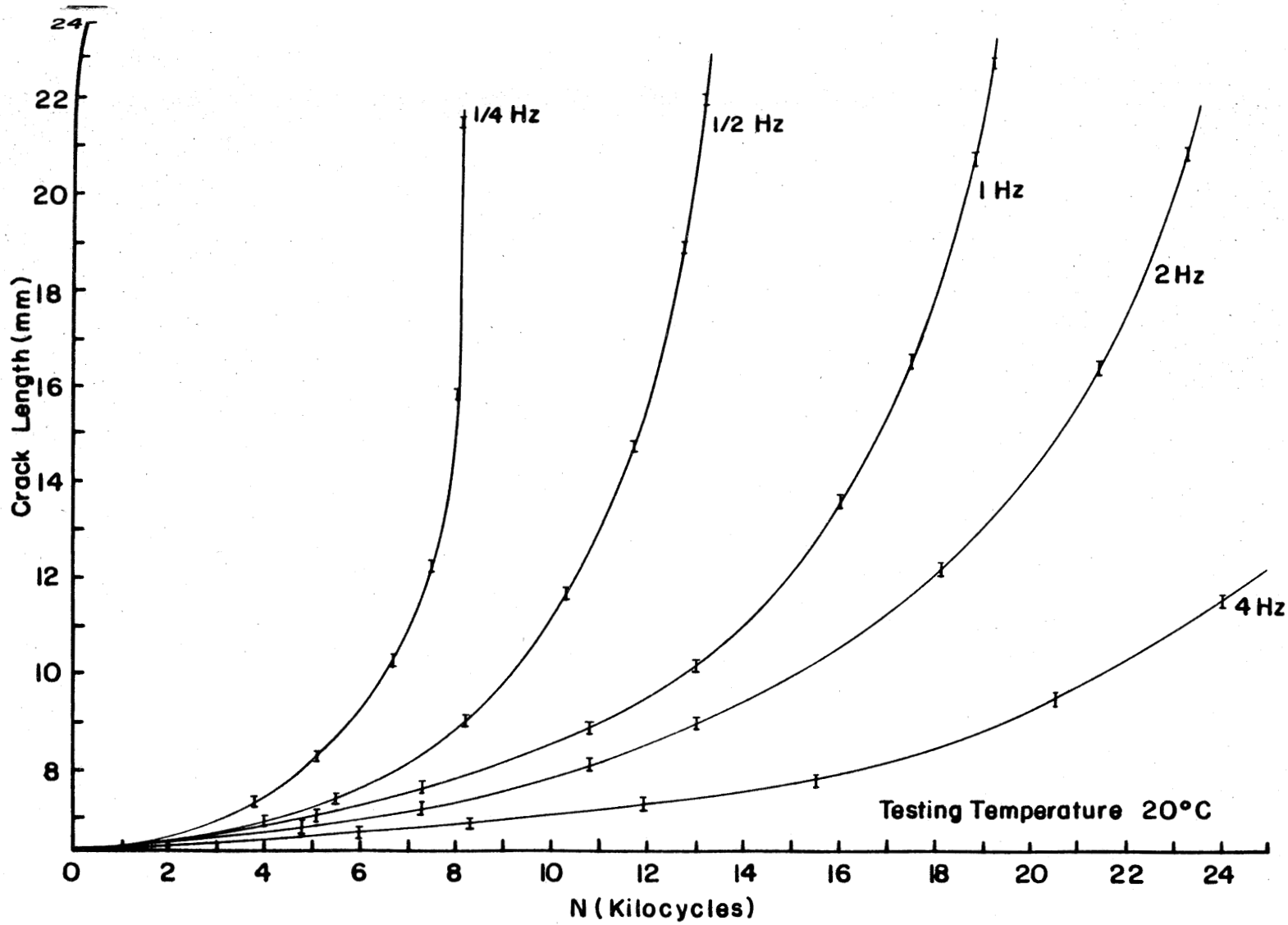


**Figure 4.3** Crack length recorded as a function of the number of cycles under different loading frequencies.

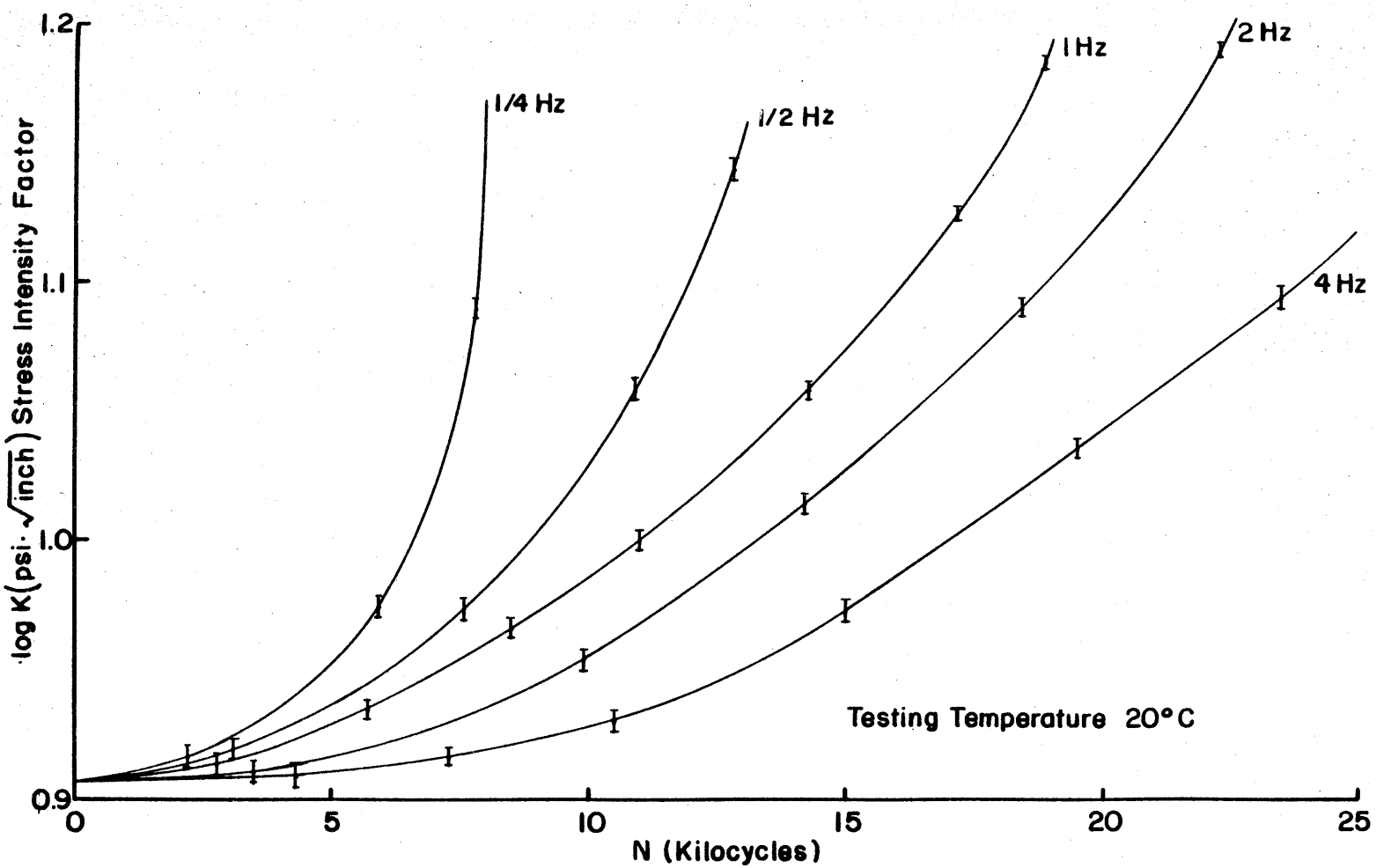


**Figure 4.4** The log values of stress intensity factor $K_I$ recorded as a function of the number of cycles under different loading frequencies.

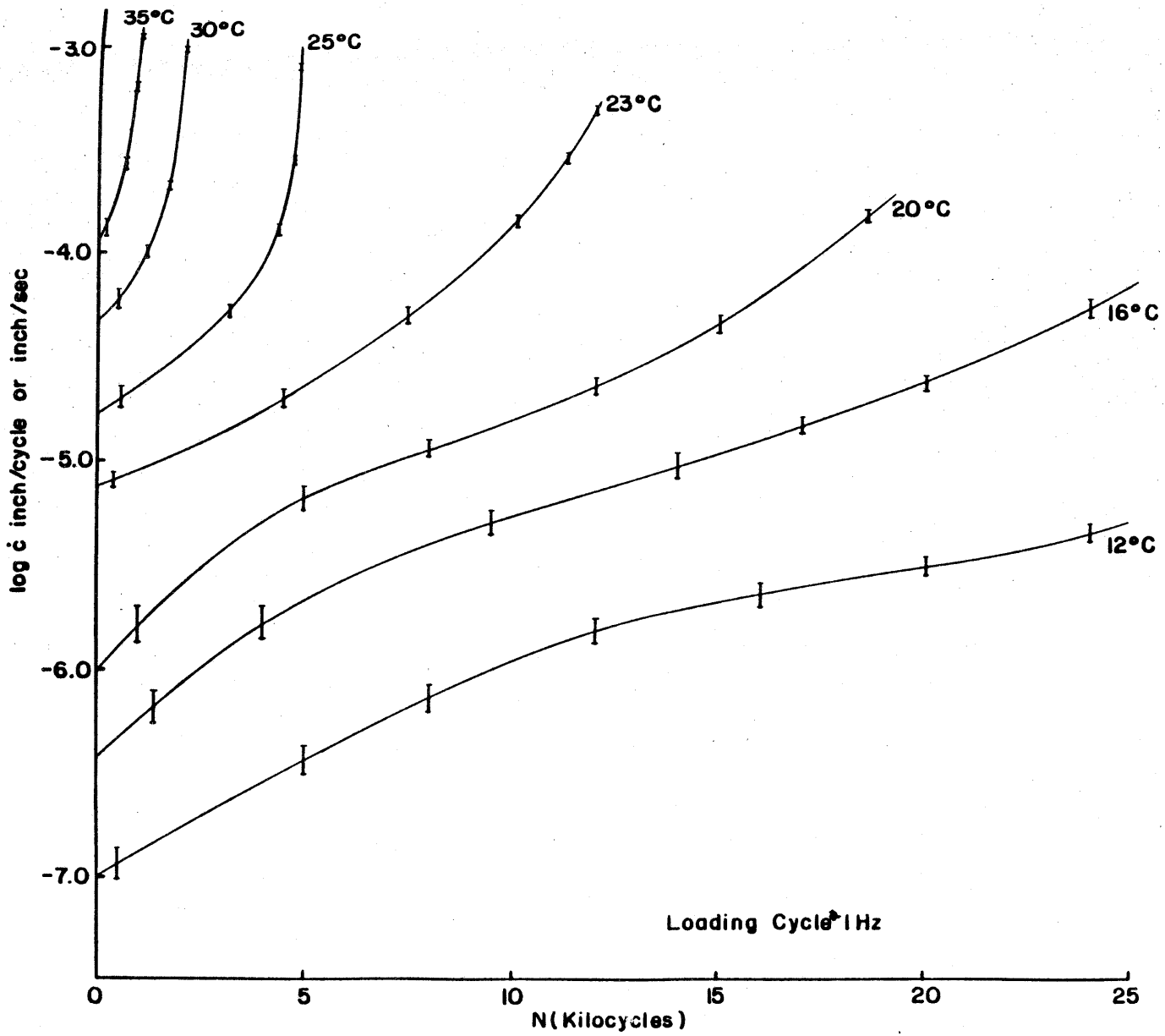


**Figure 4.5** The crack propagation speed due to change of the temperature.

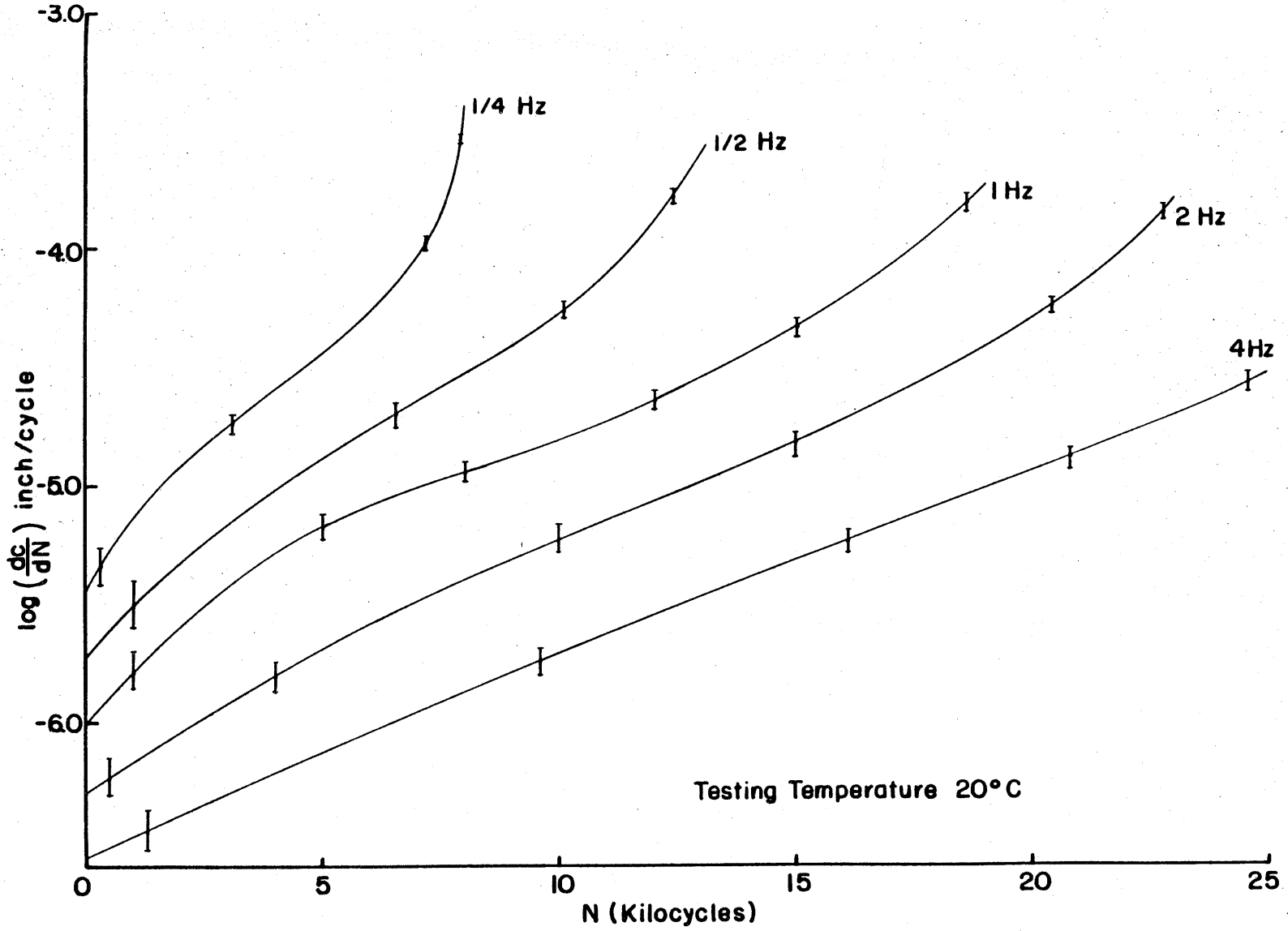


**Figure 4.6** Crack propagation speed due to change of loading frequencies.

cycle number and derives a plot of crack growth rate as a function of the maximal stress intensity factor in each cycle ($K_{max}/K_{min}$ ranges between 3.0 and 3.6 during these tests); this is shown for Set I in Figure 4.7. Similarly, if one cross plots Figures 4.4 and 4.6 one arrives at the data in Figure 4.8 for Set II. Thus Figures 4.7 and 4.8 constitute the starting data for examining the possible effect of viscoelasticity on crack propagation under transient loading.

## 5. ANALYSIS OF EXPERIMENTAL RESULTS

We notice first, with respect to Figure 4.7, that the overall behavoir of crack growth as a function of temperature is as expected from the time-temperature superposition behavior. However two deviations are rather obvious: If the data behaved strictly according to the time-temperaure superposition principle, the curves in Figure 4.7 should all have the same shape. That is clearly not the case at low (maximal) stress intensity and progressively less true as the temperature increases.

In this connection it must be remembered that stress cycling occurred between some minimum and maximum value in each cycle. In these tests the minimum value (2.5 psi) was large enough so that during most of the cycle crack propagation became possible at the higher temperature. This "anomaly" of the data in the low-K, high-T region is thus due to an effectively superposed steady stress intensity factor which makes a significant contribution only when $K_{max}$ is small ($K_{max}/K_{min} \rightarrow 3.0$) and when the temperature is such as to allow significant crack growth under this low stress condition.

The second "anomaly" becomes apparent when one time-temperature shifts the curves in Figure 4.7 or cross plots them at difference values of the stress intensity factor against temperature. This plotting is done in Figures 4.9 and 4.10. In accordance with the time-temperature behavior indicated by the dotted

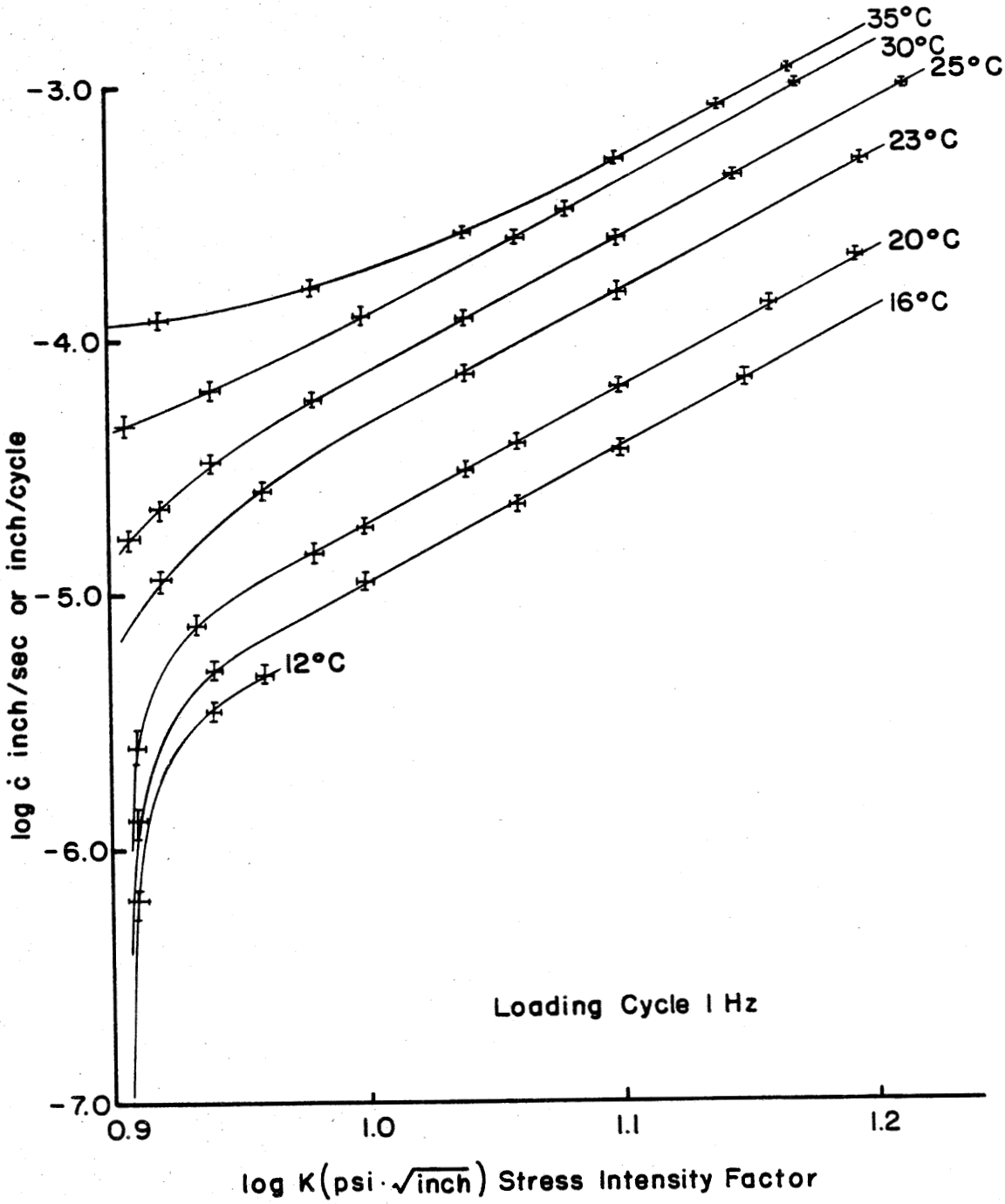


**Figure 4.7** Crack propagation rate due to change of temperature.

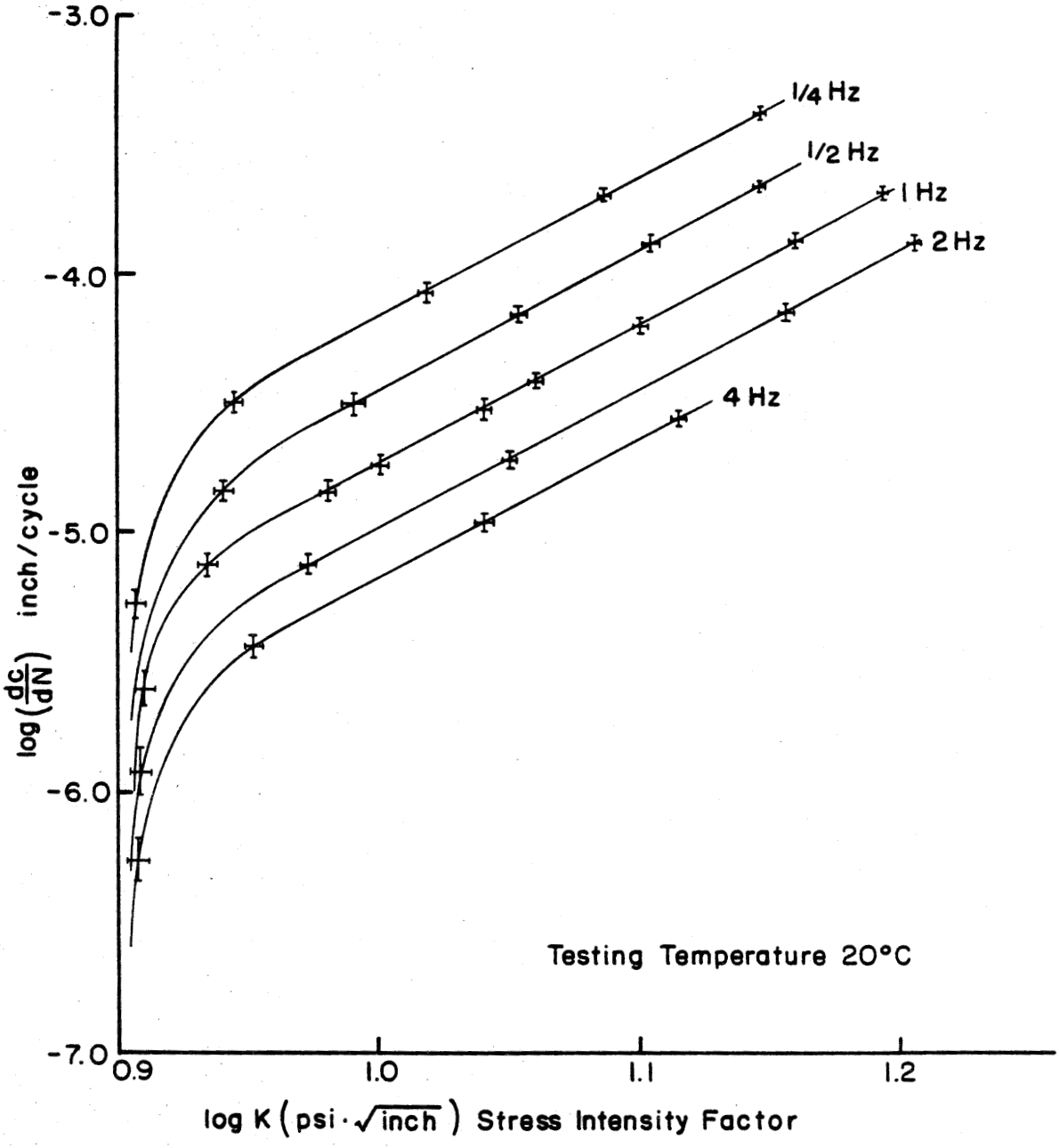


**Figure 4.8** Crack propagation rate due to change of loading frequencies.

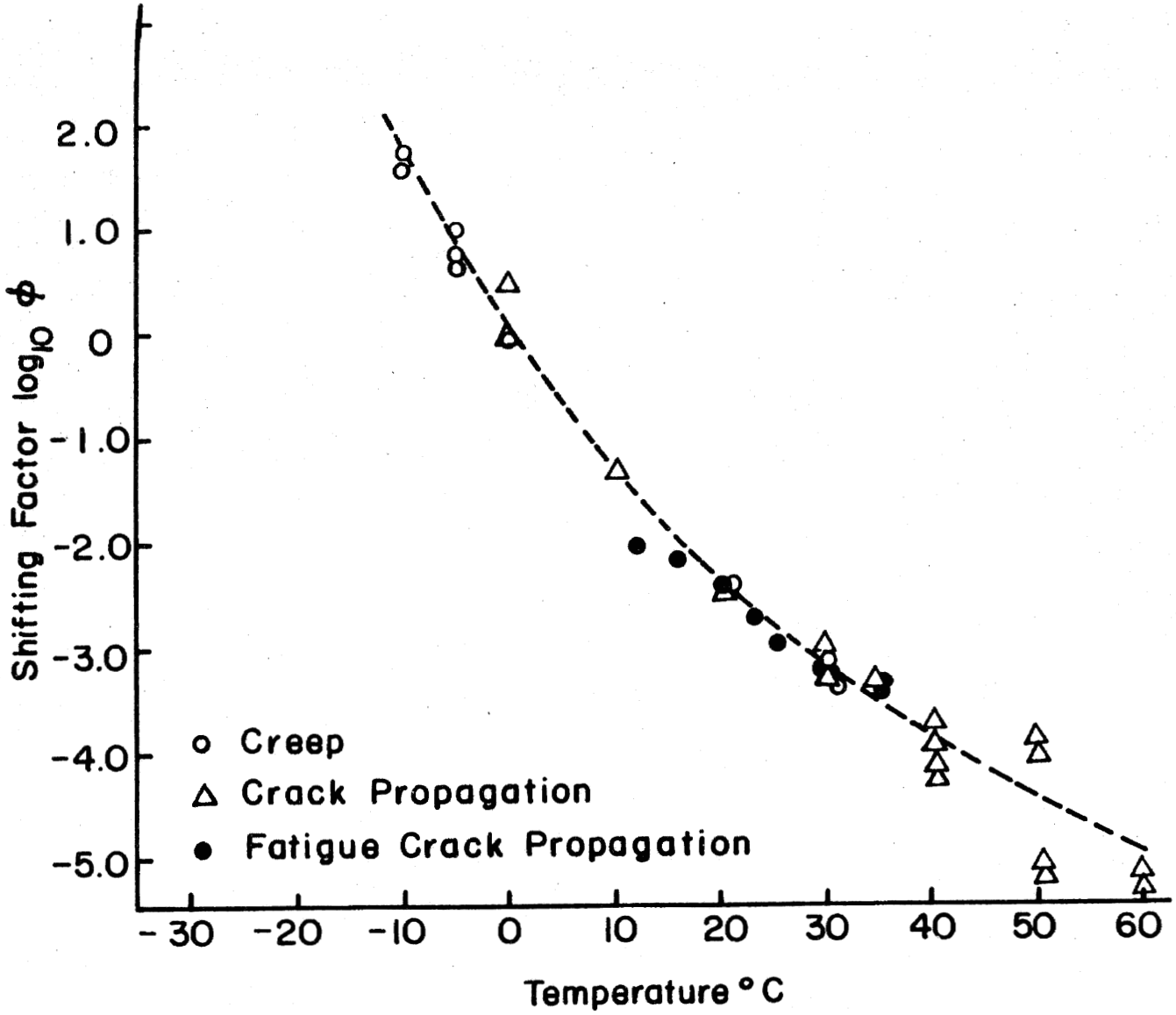


**Figure 4.9** Master curve of shifting factors.

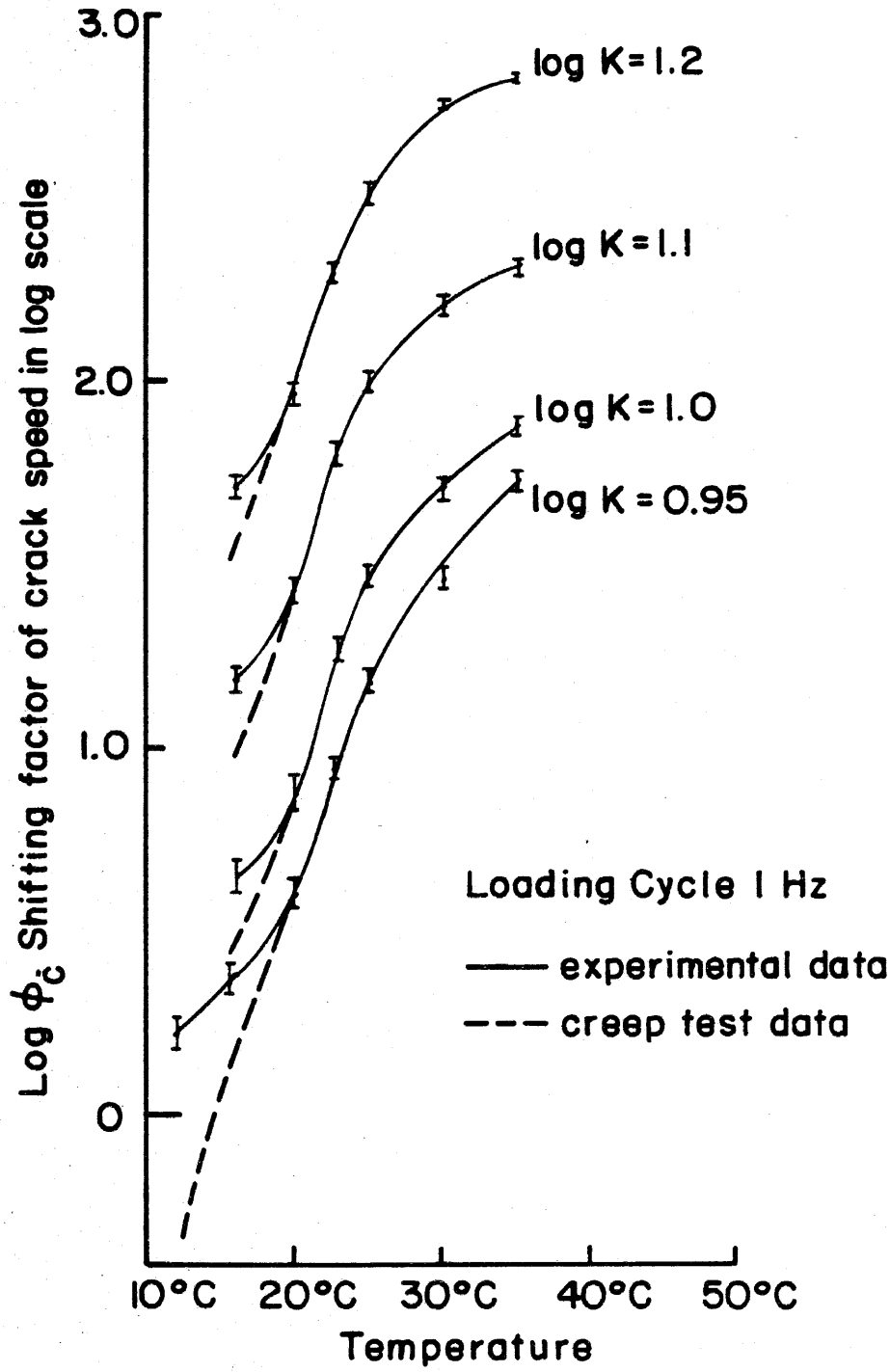


**Figure 4.10** Shifting factor of crack speed due to change of temperature.

curve[1] in Figure 4.9 the plots in Figure 3.10 should exhibit a monotonic curvature behavior as a function of temperature. The fact that this does not occur but significant deviation occurs *consistently* at the lower temperatures indicates a systematic variation of the fatigue crack growth from standard time-temperature superposition behavior. In fact the deviation is such (the dashed curves in Figure 4.9 correspond to the dotted one in Figure 4.10) that *crack propagation is higher at these low temperatures than normal* time-temperature superposition would predict. We are aware of the normal data scatter in measurements of this type, but believe that the behavior in Figure 4.10 is systematic at all stress intensities.

If one neglects these finer points, one finds that, grossly speaking the time-temperature behavior is well obeyed in these fatigue tests as long as the temperature remains above 20°C at a frequency of 1 Hz. This, more rough comparison is illustrated in Figure 4.11 which shows comparison of the K-$\dot{c}$ relation computed from equation (1) assuming quasisteady behavior (equation (1) valid instantaneously; dashed curve for 0°C, see Ref. 6). The experimental data for the present study (solid curve) agrees rather well with the computed data at 20°C (dotted curve).

Let us now examine the behavior at 20°C when the cycle frequency is changed. It is clear from Figure 4.8 that a standard plot of dc /dN against K makes the cyclic growth rate strongly dependent on frequency. It is natural to ask, therefore, whether the characterization on a "per-cycle" basis is more appropriate than on a "per-unit-time" basis.[2] After all, we have seen in Section 2 that the crack growth should, at least approximately, be predictable by a time-differential equation. Thus, if one converts the ordinate in Figure 3.8 from

1. This figure is an accumulation of data from different tests on the same material [2-4].
2. Standard fatigue data is presented on a "per cycle" basis.

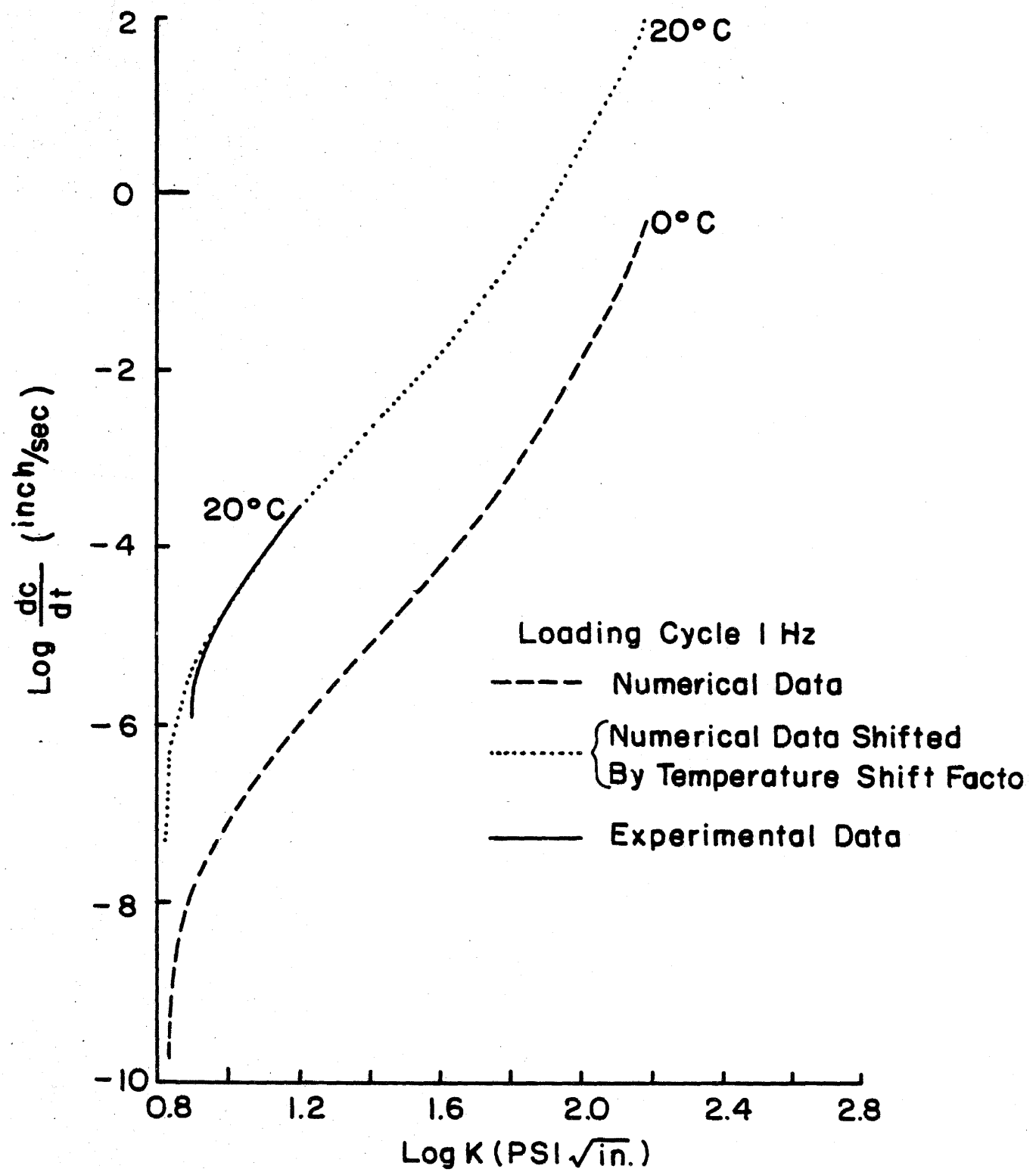


**Figure 4.11 Comparison of computed and measured crack propagation rate.**

dc /dN to dc /dt one finds in Figure 4.12 a much closer agreement, although, due primarily to the low data scatter in Figures 4.3 and 4.4, one can distinguish a systematic separation of the curves with increasing frequency. Specifically we note that ***higher frequencies lead to faster crack propagation rates*** than lower frequencies. For "low" frequencies the curves all seem to collapse into a simple master curve which should be equal to that computed from the quasi-static and monotonically-based crack propagation equation (1).

With reference to the previous test series "Set I" were low temperature produced crack growth rates that were higher than those predicted by the quasi-static theory the same is true here for higher frequency. Since higher frequency has the same effect on viscoelastic behavior as lower temperature, we conclude that ***under increased viscoelastic material response in the near-relaxed range of material behavior crack propagation is accelerated by a cyclic load history. This behavior is commensurate with the concept of fatigue.***

That the curves in Figure 4.13 do not all collapse onto a single master curve - thus attributing the separation of the curves possibly to data scatter - is evident when one cross plots the data in Figure 4.13 for constant frequencies as in Figure 4.12. If all the curves where essentially statistical variants of each other the dotted curves in Figure 4.13 should have all zero slope. It is evident that that would hardly be an appropriate interpretation and that the systematic and pronounced slope is significant, thus demonstrating the systematic variation of the crack growth rate with frequency.

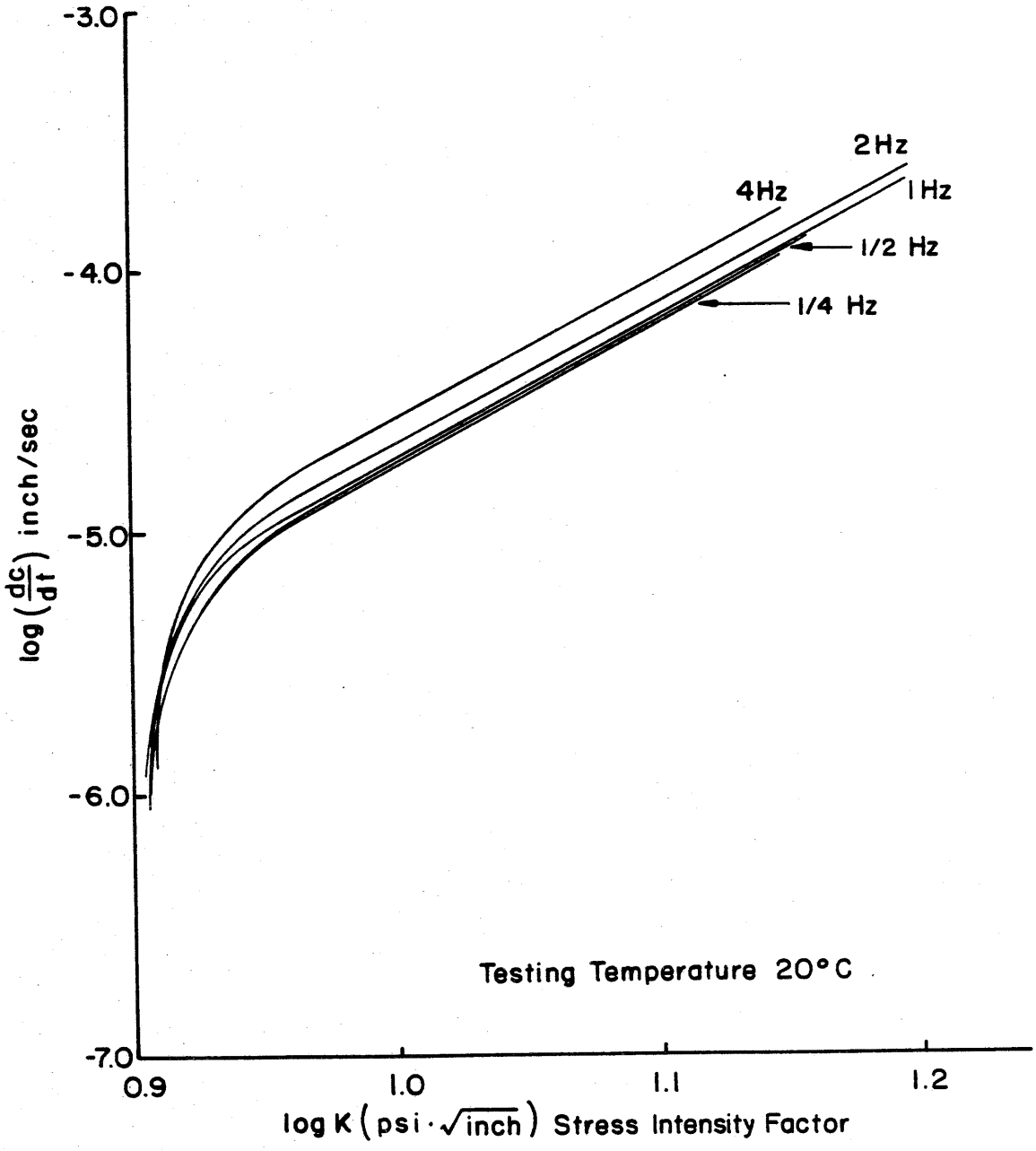


**Figure 4.12** Crack propagation rate due to change of loading frequencies.

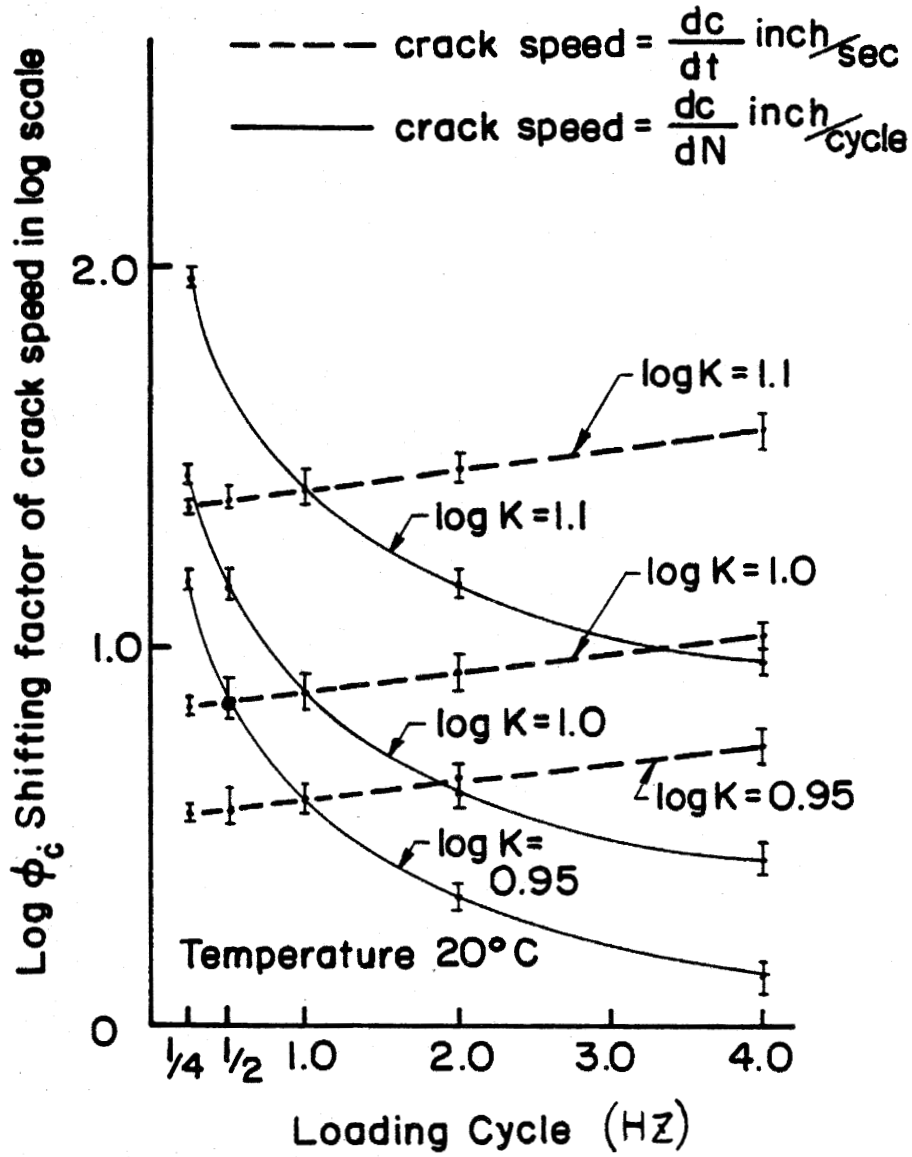


**Figure 4.13** Shifting factor of crack speed due to change of loading frequency.

**REFERENCES**


1. Knauss, W.G., and Dietmann, H. "Crack Propagation Under Variable Load Histories in Linearly Viscoelastic Solids," *Int. J. Eng. Sci.*, Vol. 8 (1970) pp. 643-656.

2. Knauss, W.G., "On the Steady Propagation of a Crack in a Viscoelastic Sheet: Experiments and Analysis." *Deformation and Fracture of High Polymers*, H.H. Kausch, J.A. Hassell and R.I. Jaffee (eds.), Plenum Press (1973).

3. Schapery, R.H., "A Theory of Crack Initiation and Growth in Viscoelastic Media; I. Theoretical Development," *Int. J. Fracture*, 11 (1975) pp. 141-159.

4. Schapery, R.H., "A Theory of Crack Initiation and Growth in Viscoelastic Media; II. Approximate Methods of Analysis," *Int. J. Fracture*, 11 (1975) pp. 369-388.

5. Knauss, W.G., "Fracture of Solids Possessing Deformation Rate Sensitive Material Properties." *The Mechanics of Fracture*, F. Erdogan (ed.) AMD-Vol. 19, Amer. Soc. of Mech. Eng. (1976)

6. von Bernstorff, Bernd-Steffen Graf, "Crack Growth in Viscoelastic Materials Under Varying Load Histories," Thesis, California Institute of Technology, 1980.

7. Kim, K.S., and Knauss, W.G., "Dynamic Fracture in Viscoelastic Solids," GALCIT SM Report 81-7 (1981).

8. Rooke, D.P., and Cartwright, D.J., "Compendium of Stress Intensity Factors," Her Majesty's Stationery Office (HMSO), London (1976).

9. Kobayashi, A.S., "Photoelasticity Techniques." *Experimental Techniques in Fracture Mechanics*, SESA No. 1 (1973).

10. Dahlquist, G., and Björck, A., "Numerical Methods." Prentice-Hall (1974).

11. Hildebrand, F.B., "Introduction to Numerical Analysis." McGraw-Hill (1956).

# APPENDICES

## APPENDIX A: ENVIRONMENTAL CONTROL

In this Appendix we describe briefly the experimental set-up with regard to temperature and frequency control. This is appropriate because relatively small changes in temperature may affect the crack propagation rate measurably and singificantly. The schematic of the interacting components are shown in Figure A-1.

### THE LOADING SYSTEM

The servo-hydraulic loading device is home built but essentially from component that normally makes up MTS equipment employing an MTS frame ratio at 22 klb. However, the maximum load applied was always less than 10 lbs., so the frame can be treated as rigid body.

A hydraulic power system with servo controler monitors and controls the loading history through a function generator with a DC offsetting sine wave of fixed frequency and maximum amplitude. Thus the loading system provided essentially amplitude (sinusoidal) displacement control to the ends of the specimen. Because of the limitations on the available cooling system the whole loading system can run continuously for up to 16 hours with steady put. The environmental chamber (Figure A-2) is a double-wall wooden container with dimensions that just fit between the MTS' frame. The testing sample, Solithane 113 strip, is located in the chamber in a steady temperature environment. With the help of a fan air circulates from a conditioning chamber into the environmental chamber (Figure A-2) which by itself is an adjustable temperature chamber. The temperature capability of this facility is in the range 100°C to 150°C (in the low temperature range cooling is accomplished with the aid of

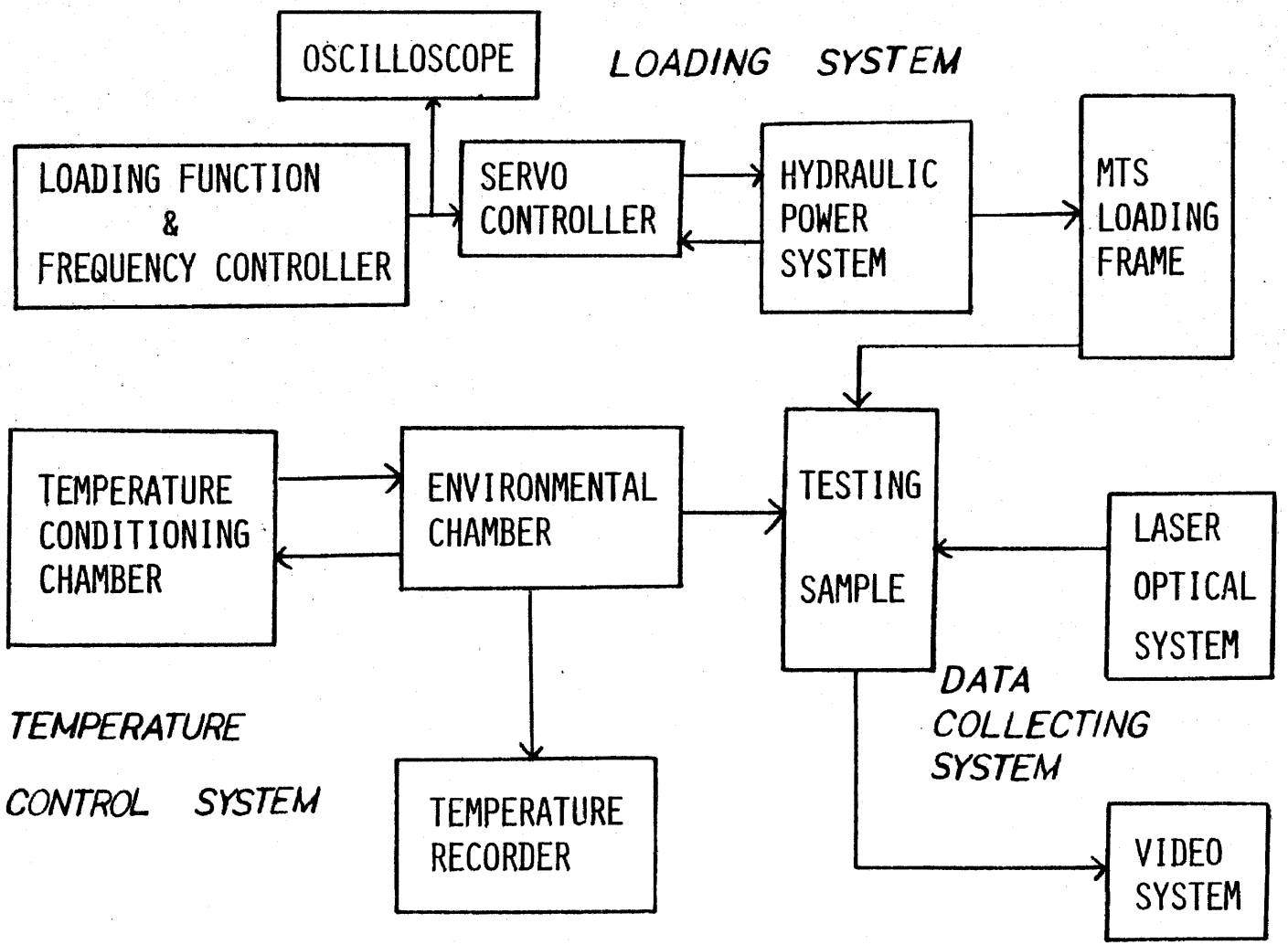


**Figure A-1** Experimental set-up.

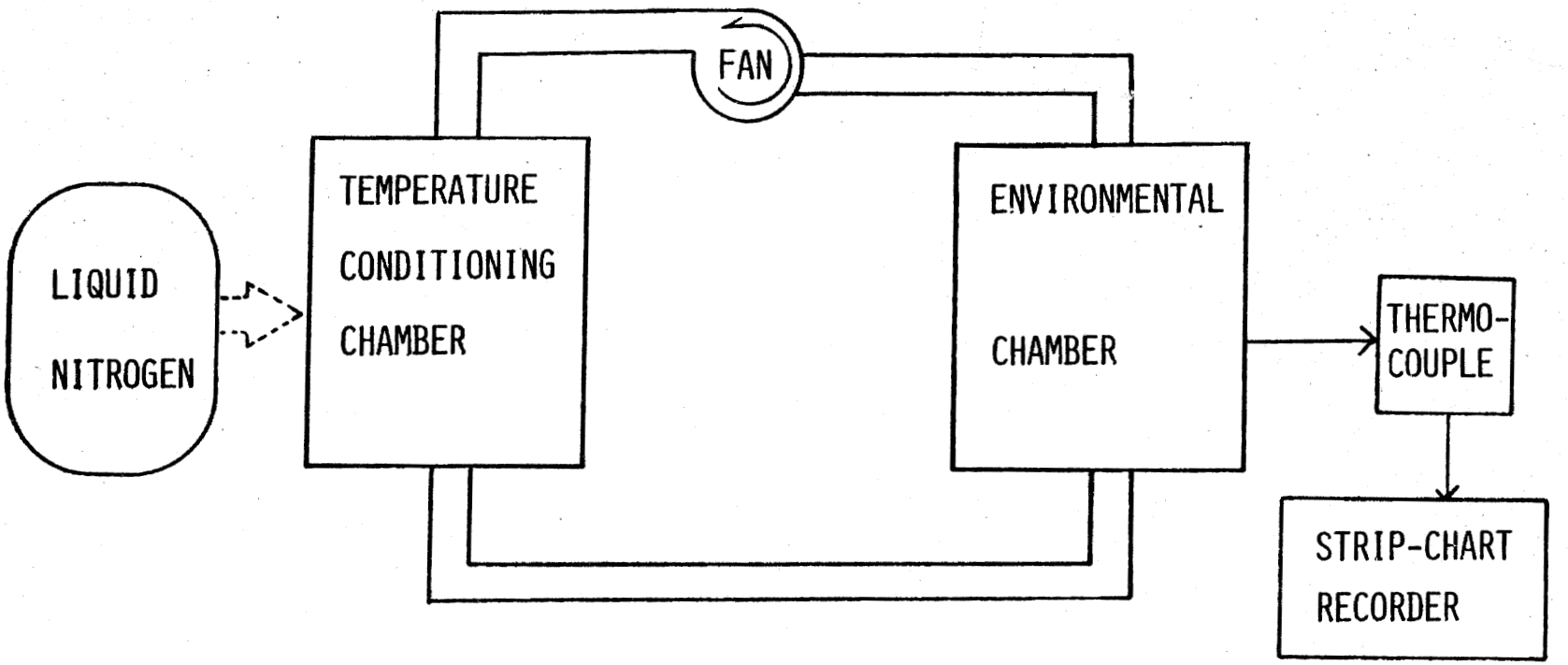


**Figure A-2** Temperature control system.

liquid Nitrogen).

Two Nickel-Chromium vs. Copper-Nickel thermo couples are placed on the surfaces of the Solithane 113 specimen and the temperature, as the output voltages from the thermo-couples, is recorded continuously on HP 7200B, a strip-chart recorder. For the range of test temperatures, $12°C \leq T \leq 35°C$, the temperature control system can maintain temperature fluctuations on the specimen surfaces to within $\pm$ 0.02 mV of the thermocouple voltage, i.e. average temperature error is $\pm$ 0.3 ~ 0.5°C. This range corresponds to approximately a variation in temperature of $\pm$ 0.4°C.

## APPENDIX B: CRACK TIP LOCATION RELATIVE TO THE CAUSTICS

On the image plane, the caustic curve is:

$$x' = r_s(\cos\varphi + \frac{2}{3}\cos(\frac{3}{2}\varphi))$$

$$y' = r_s(\sin\varphi + \frac{2}{3}\sin(\frac{3}{2}\varphi))$$

$$D = 2y'_{max}\,.$$

$$\frac{dy'}{d\varphi} = r_s(\cos\varphi + \cos(\frac{3}{2}\varphi)) \tag{A.1}$$

$$\frac{d^2y'}{d\varphi^2} = -r_s(\sin\varphi + \frac{3}{2}\sin(\frac{3}{2}\varphi)) \tag{A.2}$$

let $\frac{dy'}{d\varphi} = 0$ from (A.1) it is:

$$\frac{3}{2}\varphi = 180^\circ - \varphi \qquad \text{for } 0 \le \varphi \le 180^\circ$$

$$\varphi = 72^\circ$$

$$\frac{d^2y'}{d\varphi^2}\Big|_{\varphi=72^\circ} = -2.378\,r_o < 0$$

So it is proved that at $\varphi = 72^\circ$ $y' = y'_{max}$

$$x'\Big|_{\varphi=72^\circ} = 0.103\,r_s$$

finding $y' = 0$, i.e.,

$$\sin\varphi + \frac{2}{3}\sin(\frac{3}{2}\varphi) = 0 \qquad \varphi = 0^\circ \text{ or } 151.05^\circ$$

$$x'\Big|_{\varphi=0^\circ} = \frac{5}{3}r_s$$

$$x'\Big|_{\varphi=151.05^\circ} = -1.3333113\,r_s$$

$$\cong -\frac{4}{3}r_s$$

$$L = \left| -\frac{4}{3}r_s \right| + \left| \frac{5}{3}r_s \right| = 3r_s$$

$$\frac{\left| -\frac{4}{3}r_s \right|}{3r_s} = \frac{4}{9}$$

the position of crack tip is at $\frac{4}{9}L$. And the position of the maximal distance of the caustic from the x-axis, i.e. $Y' = \frac{D}{2}$ occurs at a distance $\bar{x}$ from the left of the caustics (see Figure 3.8).

$$\frac{\bar{x}}{L} = \frac{\frac{4}{3}r_s + 0.103r_s}{3r_s} = 0.479$$